ELSEVIER

Agricultural and Forest Meteorology 88 (1997) 215–239

AGRICULTURAL AND FOREST METEOROLOGY

Small-scale study of three-dimensional distribution of photosynthetically active radiation in a forest

Yuri Knyazikhin *, Guido Mießen, Oleg Panfyorov, Gode Gravenhorst

Institute of Bioclimatology, University Göttingen, Büsgenweg 2, D-37077 Göttingen, Germany

Received 12 August 1996; received in revised form 24 March 1997; accepted 30 April 1997

Abstract

We use the transport theory to simulate three-dimensional radiation distribution in a vegetation canopy of a small area (ca. 0.1–0.3 ha). This theory is based on two contradictory assumptions (Ross, 1981). On the one hand, the model resolution have to be so high that input variables for the transport equation can approximate the given forest stand with necessary degree of accuracy. On the other hand, the transport theory is based on the assumption that Beer's law can be locally applied to plant canopies that is valid for sufficiently large volumes filled with phytoelements. This sets a limit to the resolution and to the predicting accuracy, not only of our model, but also of any other using Beer's law. The aim of our paper is to estimate these limits as a function of input variables. A detailed analysis of input variables (canopy structure, optical properties of foliage elements and soil, radiation input at the canopy boundary) and of their effect on the radiative field underlie our investigations. A comparison of our three-dimensional simulation results with field measurements is also included in our paper, not only to test the model, but also to illustrate the specification of a model resolution and the accuracy of predicted radiative field in a real small heterogeneous experimental site.

The forest albedo is an important ecological variable characterising the forest scattering capacity. To measure this variable, two hemispherical sensors are usually mounted above the forest canopy. The first one records a downward energy flux from the atmosphere, and the second, an upward irradiance reflected by the forest. The ratio of their responses is usually interpreted as the forest albedo. As an example, the model is used to quantify an inadequacy of this interpretation by simulating both the sensor response and the three-dimensional distribution of the radiation reflected, and by comparing these results with measurements in the field. © 1997 Elsevier Science B.V.

Keywords: Transport theory; Forest; Phytoelements; Beer's law; Albedo; Radiation

1. Introduction

The incoming solar radiation triggers a complicated series of biophysiological, chemical and physical processes in a forest canopy. One of the basic phenomena responsible for the processes is the interaction between the phytoelements and the radiant energy on these phytoelements. Therefore, to quantitatively and

* Corresponding author.

PII S0168-1923(97)00036-1

correctly interpret the functioning of forests, it becomes increasingly important to thoroughly understand the interacting process of electromagnetic radiation with phytoelements.

Numerous one-dimensional canopy-radiation models have been developed since the classical model of Monsi and Saeki (1953). Most of them are based on the assumption that the forest canopy can be idealised as a horizontally homogeneous medium. This idealisation is well justified if the very general (large-scale) aspects of forest functioning of sufficiently large plant communities are investigated. For a more precise research of microphysiological processes in a given forest, a given tree, and a given time period, this treatment, however, may be inadequate. For example, stands with identical vertical foliage distribution, but differing degrees of horizontal homogeneity, can have very different radiative regime (Smith, 1993; Stenberg et al., 1994).

Great efforts have already been made by the radiative transfer community to simulate the transport and interaction of electromagnetic radiation in heterogeneous three-dimensional scenes (Norman and Welles, 1983; Ross and Marshak, 1984; Li and Strahler, 1986; Goel, 1988; Myneni et al., 1990; Borel et al., 1991; Kimes, 1991). Most of them, however, were aimed at examining the scattering behaviour of various types of vegetation and were mainly designed for optical remote sensing of vegetative scenes. The interaction of photons with the rough surface of tree crowns and with the soil in between-crown openings is the most important factor causing the observed variation in the directional reflectance distribution of plant canopies. On the contrary, the within-crown radiative regime is the most important factor determining the functioning of forests. Several models allow for internal tree structure and their effect on the within-stand and within-crown radiative regime (Oker-Blom and Kellomäki, 1983; Oker-Blom, 1986; Wang and Jarvis, 1990; Nilson, 1992; Stenberg, 1995). They, as a rule, are based on the assumption that the foliage distribution obeys some statistical laws that is a result of already existing canopy organisation. Knowledge of small-scale features of the radiative field in plant canopies, therefore, is needed to better understand the canopy organisation.

The aim of our paper is to study three-dimensional distribution of photosynthetically active radiation (PAR) in a forest of a small area (ca. 0.1–0.3 ha). The development of three-dimensional canopy-radiation models at small spatial and temporal scales is essential in achieving a better understanding of the impact of forest ecosystems on microprocesses in an individual tree and feedback mechanisms. Their advantages may be a better use of environmental resources and governing mechanisms of tree competition for light, and sustainable multifunctional forest management.

Our model is based on the three-dimensional transport equation (Ross, 1981). The radiative field is defined to be a solution of this equation in our paper. A computational technique developed in reactor physics for the numerical solution of the transport equation (Myneni et al., 1990; Knyazikhin and Marshak, 1991; Ross et al., 1992) was utilised in our model to resolve the transport equation. Therefore, we begin with a description of the radiative transfer process in terms of this equation (Section 2.1). However, we will not discuss either properties of the transport equation or methods for its resolving. The aim of this section is only to give precise definitions of all variables used in our paper. In computing the radiative field we closely follow the technique by Myneni et al. (1991).

To estimate the forest radiative regime, three important input variables must be carefully formulated (Ross, 1981). They are: (1) architecture of an individual tree and the entire canopy, (2) optical properties of the vegetation elements and soil, and (3) atmospheric conditions that determine the radiation input at the canopy boundary. Inaccuracies in these attributes can usually be compensated by averaging the predicted radiative field over large spatial and temporal scales. In investigations of small-scale features of the radiative field, such an average, however, cannot be usually performed. Inaccuracies in input variables, therefore, can essentially influence prediction results in this case. There is another problem encountered in the small-scale canopy–radiation modelling. The transport equation is based on the assumption that Beer's law can be locally utilised to describe light interaction in plant canopies. However, this law, on the average, holds true for sufficiently great volumes filled with phytoelements (Ross, 1981, p. 144; Knyazikhin et al., 1992; Larsen and Kershaw, 1996). Two types of inaccuracies, therefore, must be considered to predict the small-scale radiative field in forest canopies correctly: the inaccuracies in input variables, and the inaccuracy of prediction capacity of Beer's law.

Increasing the accuracy of input variables does not lead to improving the accuracy of Beer's law. It sets a limit to an applicability range of the transport theory. It is also our aim to estimate this limit. In Section 2.2, we introduce a concept of a model quality and of a model resolution to quantify the aforementioned inaccuracies. Sections 3–5 focus on the analysis of the accuracy and quality of the input variables and their effect on the radiative field in forest canopies of a small area.

The forest albedo, defined as the ratio of the total solar energy reflected by the forest to the one incident at the forest, is an important ecological variable characterising the forest scattering capacity. To measure this variable, two hemispherical sensors are usually mounted above the forest canopy. The first one records a downward energy flux from the atmosphere, and the second, an upward irradiance reflected by the forest. The ratio of their responses is usually interpreted as the forest albedo. In Section 6, we utilise our model to quantify an inadequacy of this interpretation by simulating both the sensor response and the three-dimensional distribution of the radiation reflected, and by comparing these results with measurements in the field.

A comparison of our three-dimensional simulation results with field measurements is also a focus of the present paper, not only to test the model, but also to specify the quality of input variables required to provide a correct simulation of the radiative field in a small heterogeneous forest stand. These results are included in Section 3.

2. Radiation transport

2.1. Boundary value problem for the transport equation

We consider a forest canopy consisting of some individual trees. The domain V, in which the trees are located is a parallelepiped of dimension X_S, Y_S and Z_S. The height, Z_S, of the forest canopy coincides with the maximum tree height. The top (δV_t), bottom (δV_b) and lateral (δV_l) surfaces of the parallelepiped form the canopy boundary, $\delta V = \delta V_t + \delta V_b + \delta V_l$. Note the boundary, δV, is excluded from the definition of V. The function characterising the radiative field is the monochromatic intensity distribution function, $I_\lambda(\boldsymbol{r},\boldsymbol{\Omega})$, depending on wavelength, λ (in m), location $\boldsymbol{r} = (x,y,z)$ and direction $\boldsymbol{\Omega}$. Under condition of the absence of polarisation, frequency shifting interaction, and emission processes within the canopy, the monochromatic intensity distribution function is given by the steady-state radiative transfer equation (Ross, 1981; Myneni et al., 1990; Myneni, 1991):

$$\boldsymbol{\Omega}\cdot\nabla I_\lambda(\boldsymbol{r},\boldsymbol{\Omega}) + \sigma(\boldsymbol{r},\boldsymbol{\Omega})I_\lambda(\boldsymbol{r},\boldsymbol{\Omega}) = \int_{4\pi}\sigma_{S,\lambda}(\boldsymbol{r},\boldsymbol{\Omega}'\rightarrow\boldsymbol{\Omega})I_\lambda(\boldsymbol{r},\boldsymbol{\Omega}')\mathrm{d}\boldsymbol{\Omega}' \tag{1}$$

The position vector $\boldsymbol{r}$ denotes the triplet (x,y,z) with $(0<x<X_S)$, $(0<y<Y_S)$ and $(0<z<Z_S)$ and is expressed in Cartesian coordinates with its origin, $O=(0,0,0)$, at the top of the forest canopy and the Z axis directed down into the forest canopy. The unit vector $\boldsymbol{\Omega}\sim(\mu,\phi)$ has an azimuthal angle ϕ measured in the (XY) plane from the positive X axis in a counterclockwise fashion and a polar angle $\theta=\cos\mu$ with respect to the polar axis that is opposite to the Z axis. $\boldsymbol{\Omega}\cdot\nabla I_\lambda(\boldsymbol{r},\boldsymbol{\Omega})$ is a derivative at $\boldsymbol{r}$ along the direction $\boldsymbol{\Omega}$.

The function $\sigma(\boldsymbol{r},\boldsymbol{\Omega})$ (in m^{-1}) is the total interaction cross-section (and it does not depend on wavelength!) and $\sigma_{S,\lambda}(\boldsymbol{r},\boldsymbol{\Omega}'\rightarrow\boldsymbol{\Omega})$ the differential scattering cross-section for scattering from the direction $\boldsymbol{\Omega}'$ into a differential solid angle about $\boldsymbol{\Omega}$ at $\boldsymbol{r}$, (in $\mathrm{m}^{-1}\ \mathrm{sr}^{-1}$). In the canopy transport theory, these coefficients are defined as (Ross, 1981; Myneni, 1991):

$$\sigma(\boldsymbol{r},\boldsymbol{\Omega}) = u_L(r)G(\boldsymbol{r},\boldsymbol{\Omega}) = u_L(\boldsymbol{r})\frac{1}{2\pi}\int_{2\pi^+} g_L(\boldsymbol{r},\boldsymbol{\Omega}_L)|\boldsymbol{\Omega}\cdot\boldsymbol{\Omega}_L|\mathrm{d}\boldsymbol{\Omega}_L, \tag{2}$$

$$\sigma_{S,\lambda}(\boldsymbol{r},\boldsymbol{\Omega}'\to\boldsymbol{\Omega}) = u_L(\boldsymbol{r})\frac{1}{\pi}\Gamma_\lambda(\boldsymbol{r},\boldsymbol{\Omega}'\to\boldsymbol{\Omega}), \tag{3}$$

$$\Gamma_\lambda(\boldsymbol{r},\boldsymbol{\Omega}'\to\boldsymbol{\Omega}) = \frac{1}{2}\int_{2\pi^+} g_L(\boldsymbol{r},\boldsymbol{\Omega}_L)|\boldsymbol{\Omega}'\cdot\boldsymbol{\Omega}_L|\gamma_{L,\lambda}(\boldsymbol{r},\boldsymbol{\Omega}_L,\boldsymbol{\Omega}'\to\boldsymbol{\Omega})\mathrm{d}\boldsymbol{\Omega}_L, \tag{4}$$

where $u_L(\boldsymbol{r})$ (in m^{-1}) is the leaf area density distribution function; $G(\boldsymbol{r},\boldsymbol{\Omega})$ (dimensionless) is the mean projection of leaf normals at $\boldsymbol{r}$ onto a plane perpendicular to the direction $\boldsymbol{\Omega}$; $g_L(\boldsymbol{r},\boldsymbol{\Omega}_L)$ is the probability density of the leaf's normal distribution over the upper hemisphere $2\pi^+$; $\gamma_{L,\lambda}(\boldsymbol{r},\boldsymbol{\Omega}_L,\boldsymbol{\Omega}'\to\boldsymbol{\Omega})$ (in sr^{-1}) is the leaf scattering phase function and Γ_λ is the area scattering phase function (Ross, 1981). The precise description of these variables can be found in the literature (Ross, 1981; Myneni, 1991; Myneni et al., 1991). In our paper we closely follow the formulation of the above mentioned variables by Myneni et al., 1991.

Eq. (1) alone does not provide a full description of the transport process. It is necessary to specify the incident radiance at the canopy boundary, δV, i.e., specification of the boundary conditions. Because our forest canopy adjoins the atmosphere, a neighbouring forest and the soil having different reflection properties, the following boundary conditions will be used in our model to describe the incoming radiation (Ross et al., 1992):

$$I_\lambda(\boldsymbol{r}_t,\boldsymbol{\Omega}) = T_{d,\lambda}(\boldsymbol{r}_t,\boldsymbol{\Omega}) + T_{m,\lambda}(\boldsymbol{r}_t)\delta(\boldsymbol{\Omega}-\boldsymbol{\Omega}_0),\ \boldsymbol{r}_t\in\delta V_t, \boldsymbol{\Omega}\cdot n_t<0, \tag{5}$$

$$I_\lambda(\boldsymbol{r}_l,\boldsymbol{\Omega}) = \int_{\boldsymbol{\Omega}'\cdot n_l>0}\rho_{\lambda,l}(\boldsymbol{\Omega}',\boldsymbol{\Omega})I_\lambda(\boldsymbol{r}_l,\boldsymbol{\Omega}')|\boldsymbol{\Omega}'\cdot n_l|\mathrm{d}\boldsymbol{\Omega}' + L_{d,\lambda}(\boldsymbol{r}_l,\boldsymbol{\Omega}) + L_{m,\lambda}(\boldsymbol{r}_l)\delta(\boldsymbol{\Omega}-\boldsymbol{\Omega}_0),$$

$$\boldsymbol{r}_l\in\delta V_l, \boldsymbol{\Omega}\cdot n_l<0, \tag{6}$$

$$I_\lambda(\boldsymbol{r}_b,\boldsymbol{\Omega}) = \int_{\boldsymbol{\Omega}'\cdot n_b>0}\rho_{\lambda,b}(\boldsymbol{\Omega}',\boldsymbol{\Omega})I_\lambda(\boldsymbol{r}_b,\boldsymbol{\Omega}')|\boldsymbol{\Omega}'\cdot n_b|\mathrm{d}\boldsymbol{\Omega}',\ \boldsymbol{r}_b\in\delta V_b, \boldsymbol{\Omega}\cdot n_b<0, \tag{7}$$

where $T_{d,\lambda}$ and $T_{m,\lambda}$ are intensities of the diffuse and the monodirectional components of solar radiation incident at the top surface of the forest boundary, δV_t; $\boldsymbol{\Omega}_0\sim(\mu_0,\phi_0)$ is the direction of the monodirectional solar component; δ is the Dirac delta function; $L_{m,\lambda}(\boldsymbol{r}_l)$ is the intensity of photons in the monodirectional solar radiation arriving at a point $\boldsymbol{r}_l\in\delta V_l$ on the lateral surface, δV_l, along $\boldsymbol{\Omega}_0$ without experiencing a collision with neighbouring forest; $L_{d,\lambda}$ is the intensity of diffuse radiation penetrating through the lateral surface, δV_l, in the stand; $\rho_{\lambda,l}$ and $\rho_{\lambda,b}$ (in sr^{-1}) are the bidirectional reflectance factors of the lateral and the bottom surfaces; n_t, n_l and n_b are the outward normals at points $\boldsymbol{r}_l\in\delta V_t$, $\boldsymbol{r}_l\in\delta V_l$ and $\boldsymbol{r}_b\in\delta V_b$.

We represent the solution of Eq. (1) as the sum of two components (Ross et al., 1992), viz. $I_\lambda(\boldsymbol{r},\boldsymbol{\Omega}) = I_{m,\lambda}(\boldsymbol{r},\boldsymbol{\Omega}) + I_{d,\lambda}(\boldsymbol{r},\boldsymbol{\Omega})$, where $I_{m,\lambda}$ and $I_{d,\lambda}$ are the intensities of direct (monodirectional) and diffuse radiation, respectively. The intensity of direct solar radiation is $I_{m,\lambda}(\boldsymbol{r},\boldsymbol{\Omega}) = Q_{0,\lambda}(\boldsymbol{r})\delta(\boldsymbol{\Omega}-\boldsymbol{\Omega}_0)$, where $Q_{0,\lambda}(\boldsymbol{r})$ is the probability density that a photon in the direct solar radiation will arrive at $\boldsymbol{r}$ along $\boldsymbol{\Omega}_0$ without experiencing a collision (Myneni, 1991; Knyazikhin et al., 1994), and it may be expressed as:

$$Q_{0,\lambda}(\boldsymbol{r}) = B_{m,\lambda}(\boldsymbol{r}-l[\boldsymbol{r},\boldsymbol{\Omega}_0]\boldsymbol{\Omega}_0)\exp\left(-\int_0^{l[\boldsymbol{r},\boldsymbol{\Omega}_0]}\sigma(\boldsymbol{r}-s\boldsymbol{\Omega}_0,\boldsymbol{\Omega}_0)\mathrm{d}s\right) \tag{8}$$

Here $B_{m,\lambda}(\boldsymbol{r})$ is the function defined on the canopy boundary, δV, as:

$$B_{m,\lambda}(\boldsymbol{r}) = \begin{cases} T_{m,\lambda}(\boldsymbol{r}), & \text{if } \boldsymbol{r}\in\delta V_t,\\ L_{m,\lambda}(\boldsymbol{r}), & \text{if } \boldsymbol{r}\in\delta V_l,\\ 0, & \text{if } \boldsymbol{r}\in\delta V_b \end{cases} \tag{9}$$

that may be interpreted as the intensity of direct solar radiation penetrating through the boundary, $\delta V_t + \delta V_l$, into the forest; $l[\boldsymbol{r},\boldsymbol{\Omega}]$ denotes the distance between the point $\boldsymbol{r}$ and the forest boundary along the direction $-\boldsymbol{\Omega}$ (i.e., the point $\boldsymbol{r} - l[\boldsymbol{r},\boldsymbol{\Omega}]\boldsymbol{\Omega}$ belongs to the canopy boundary δV).

The intensity of diffuse radiation satisfies the integro-differential equation in V

$$\boldsymbol{\Omega}\cdot\nabla I_{\mathrm{d},\lambda}(\boldsymbol{r},\boldsymbol{\Omega}) + \sigma(\boldsymbol{r},\boldsymbol{\Omega}) I_{\mathrm{d},\lambda}(\boldsymbol{r},\boldsymbol{\Omega}) = \int_{4\pi} \sigma_{\mathrm{S},\lambda}(\boldsymbol{r},\boldsymbol{\Omega}'\to\boldsymbol{\Omega}) I_{\mathrm{d},\lambda}(\boldsymbol{r},\boldsymbol{\Omega}')\mathrm{d}\boldsymbol{\Omega}' + \sigma_{\mathrm{S},\lambda}(\boldsymbol{r},\boldsymbol{\Omega}_0\to\boldsymbol{\Omega}) Q_{0,\lambda}(\boldsymbol{r}), \tag{10}$$

and the boundary conditions on the forest boundary δV:

$$I_{\mathrm{d},\lambda}(\boldsymbol{r}_t,\boldsymbol{\Omega}) = T_{\mathrm{d},\lambda}(\boldsymbol{r}_t,\boldsymbol{\Omega}),\ \boldsymbol{r}_t\in\delta V_t, \boldsymbol{\Omega}\cdot n_t < 0, \tag{11}$$

$$I_{\mathrm{d},\lambda}(\boldsymbol{r}_l,\boldsymbol{\Omega}) = \int_{\boldsymbol{\Omega}'\cdot n_l>0} \rho_{\lambda,l}(\boldsymbol{\Omega}',\boldsymbol{\Omega}) I_{\mathrm{d},\lambda}(\boldsymbol{r}_l,\boldsymbol{\Omega}')|\boldsymbol{\Omega}'\cdot n_l|\mathrm{d}\boldsymbol{\Omega}' + L_{\mathrm{d},\lambda}(r_l,\boldsymbol{\Omega}) + \rho_{\lambda,l}(\boldsymbol{\Omega}_0,\boldsymbol{\Omega}) Q_{0,\lambda}(\boldsymbol{r}_l)|\boldsymbol{\Omega}_0\cdot n_l| H(\boldsymbol{\Omega}_0\cdot n_l),\ \boldsymbol{r}_l\in\delta V_l, \boldsymbol{\Omega}\cdot n_l<0 \tag{12}$$

$$I_{\mathrm{d},\lambda}(\boldsymbol{r}_b,\boldsymbol{\Omega}) = \int_{\boldsymbol{\Omega}'\cdot n_b>0} \rho_{\lambda,b}(\boldsymbol{\Omega}',\boldsymbol{\Omega}) I_{\mathrm{d},\lambda}(\boldsymbol{r}_b,\boldsymbol{\Omega}')|\boldsymbol{\Omega}'\cdot n_b|\mathrm{d}\boldsymbol{\Omega}' + \rho_{\lambda,b}(\boldsymbol{\Omega}_0,\boldsymbol{\Omega})|\boldsymbol{\Omega}_0\cdot n_b| Q_{0,\lambda}(r_b),\ \boldsymbol{r}_b\in\delta V_b, \boldsymbol{\Omega}\cdot n_b<0 \tag{13}$$

where $H(a)$ is the Heaviside function whose value is 1 if $a>0$, and 0 otherwise.

In radiation measurements, it is also conventional to use the photon intensity distribution function, $I_{\lambda,\mathrm{p}}(\boldsymbol{r},\boldsymbol{\Omega})$ (in mol m^{-3} s^{-1} sr^{-1}), instead of the intensity distribution function, $I_\lambda(\boldsymbol{r},\boldsymbol{\Omega})$ (in W m^{-3} sr^{-1}). They are related by $I_\lambda(\boldsymbol{r},\boldsymbol{\Omega}) = (hc/\lambda)N_A I_{\lambda,\mathrm{p}}(\boldsymbol{r},\boldsymbol{\Omega})$ where hc/λ is the energy of one photon (in J); $h = 6.626176\cdot 10^{-34}$ J s (Planck's constant); $c = 2.99792458\cdot 10^8$ m s^{-1} (the vacuum speed of light); and $N_A = 6.02205\cdot 10^{23}$ mol^{-1} (Avogadro's constant). Eqs. (1), (5)–(7) are also valid for the photon intensity, $I_{\lambda,\mathrm{p}}(\boldsymbol{r},\boldsymbol{\Omega})$, but its unit is expressed in mol m^{-3} s^{-1} sr^{-1}. Because some of our measuring equipments register the radiation fluxes in μmol m^{-2} s^{-1}, the symbol $I_\lambda(\boldsymbol{r},\boldsymbol{\Omega})$ will denote, depending on the situation, the photon intensity or the intensity distribution function in our paper. We will also use 'radiation intensity', referring it to $I_{\lambda,\mathrm{p}}(\boldsymbol{r},\boldsymbol{\Omega})$ or $I_\lambda(\boldsymbol{r},\boldsymbol{\Omega})$.

2.2. Spatial and angular discretization; quality of input and output data

We approximate the angular dependence by discretizing the angular variable $\boldsymbol{\Omega}$ into a finite number of discrete directions. The angular-dependent variables, therefore, can take on a finite number of values in our model. Such an approach is known in the literature as the discrete ordinate method (Bass et al., 1986; Myneni et al., 1991) and has the following interpretation: photons are restricted to travel only along a finite number of discrete directions. We use the Carlson quadrature rule over the unit sphere with equal weights (Carlson, 1970) to generate such directions.

To approximate the spatial variable, we introduce a fine-spatial mesh by dividing V into fine cells $P_{i,j,k}$ of cell volume $\Delta x\Delta y\Delta z$, $\Delta x = X_S/N_x$, $\Delta y = Y_S/N_y$, $\Delta z = Z_S/N_z$:

$$P_{i,j,k} = \{(x,y,z)|(i-1)\Delta x\le x<i\Delta x; (j-1)\Delta y\le y<j\Delta y; (k-1)\Delta z\le z<k\Delta z\},\ i=1,2,\ldots,N_x;\ j=1,2,\ldots,N_y, k=1,2,\ldots,N_z. \tag{14}$$

All quantities occurring in the transport problem are assumed to be piecewise constant with respect to the spatial variable and can take new values only at the cell boundaries, which are usually mean values of these quantities over the cell volume.

Predicted radiation in one cell can greatly differ from the measured one due to mistakes in input data. Because the transport equation assumes an energy balance for any elementary volume, some other cells in the neighbourhood may exist to compensate for this difference. So the mean predicted flux over cells from this neighbourhood will, much better, agree with the mean measured fluxes over the same neighbourhood. Therefore, we introduce a P-volume model accuracy as follows. We define a domain P (e.g., geometrical figure like a sphere or a parallelepiped) of a given size. The P-volume model accuracy at space point $\boldsymbol{r}$ is an accuracy of mean predicted quantities obtained by averaging over $\boldsymbol{r}+P=\{\boldsymbol{r}'|\boldsymbol{r}'=\boldsymbol{r}+p, p\in P\}$ around the point $\boldsymbol{r}$ (the integral of the predicted quantity over $\boldsymbol{r}+P$ divided by the volume of P).

Our definition of the model accuracy depends on the choice of P: various P's can provide various volume model accuracies. A domain P which provides an acceptable P-volume accuracy is defined to be the P-model quality. We say that a model has an ideal quality if any P is the P-model quality. We will carry out in detail the quality analysis of our model in Section 3.

The volume model accuracy depends, to a great degree, on the number of fine cells in P. To quantify this property we introduce a model resolution as the ratio between the total amount of cells in V and its volume, i.e.,

$$A=\frac{N_x N_y N_z}{X_S Y_S Z_S}=\frac{1}{\Delta x\Delta y\Delta z},$$

in fine cells/m^3.

Thus, we use two attributes to describe the model accuracy. They are the P-model quality and the model resolution. The domain P defines the neighbourhood of each space point $\boldsymbol{r}$, i.e., we consider both the space point and the space around this point limited by P. The resolution, A, determines the number of fine cells in P around a space point $\boldsymbol{r}$, which influences the mean predicted quantities over P around the space point. In analogy to the way it was done above, we define the P-volume accuracy and the P-quality for input variables (2)–(4). We say that an input variable is ideally exact if any P provides an acceptable volume accuracy.

In linear transport theory, the accuracy in the numerical solution of the transport Eq. (1) increases linearly with the increase in the resolution of input data (Germogenova, 1986). This is a logical consequence of one of the basic assumptions of this theory: the number of scattering centres (e.g., number of leaves) in an elementary volume (in a fine cell) is proportional to this volume. This property holds true for a wide range of data resolution in nuclear and atmospheric physics problems. Theoretically, we can achieve the ideal model quality in this case by decreasing the size of P, and by increasing the model resolution. In computing the canopy radiative regime, this assumption, however, loses its validity (Ross, 1981) when data resolution becomes comparable with the size of phytoelements. Moreover, the relation between the elementary volume and the number of scattering centres in it becomes nonlinear (Zeide and Pfeifer, 1991; Vedyushkin, 1995). It sets a limit to the model resolution: after exceeding a critical resolution, instabilities in the numerical solution of the transport equation arise (Kranigk, 1996). Therefore, the choice of the model resolution needs special attention (Ross, 1981). On the one hand, the model resolution has to be so high that the input variables can approximate the given forest stand with the necessary degree of accuracy. On the other hand, it should not exceed a critical value. An appropriate model resolution will be specified by comparing simulation results with field measurements in Section 3.

3. Canopy structure

3.1. Leaf area density

The leaf area density distribution function is an important structural characteristic for a forest canopy that influences in a high degree of the radiative field in the vegetation. This function can be simulated once the architecture of individual trees and their distribution on the ground are available. Therefore, the problem of describing the leaf distribution in the forest space may be reduced to modelling the architecture of individual

tree. Three-dimensional models that take into account various features of tree architecture have been a highly active research field in recent years (Borel-Donohue, 1988; de Reffye et al., 1991; Kranigk and Gravenhorst, 1993; Kranigk et al., 1994; Kurth, 1994) and they have already been incorporated with radiation models (Borel-Donohue, 1988; Myneni et al., 1991; Knyazikhin et al., 1996; Kranigk, 1996). Although our approach can simulate the complicated three-dimensional heterogeneity of a natural forest canopy (Knyazikhin et al., 1996), we will analyse models of forest structure that considers only the tree shape and vertical distribution of foliage elements within each individual tree. Such models are still widely used and it is the aim of this paper to specify their quality, accuracy and the range of their applicability.

A coniferous (*Picea abies* (L.) Karst) stand in Solling ca. 50 km Northwest of Göttingen, Germany, was chosen for simulation ('F1 Fläche', 52.77°N, 9.58°E). This forest is about 110 yrs old. A site covering an area of 25×30 m^2 was selected for our investigation. There were 35 trees in the sample stand (corresponding to a tree density of 467 trees/ha). The trees are, on the average, 29 m in height with the crown height of about 11 m. Thus, V, where the trees are located, is the parallelepiped of dimensions $X_S = 25$ m, $Y_S = 30$ m and $Z_S = 29$ m. The coordinate system is aligned such that the angle between the positive X axis and the direction to the north is 75°. The projection of the tree crowns is shown in Fig. 1. A coniferous one-year shoot of size 5–7 cm with needles was considered to be the basic foliage element in our model.

The vertical density distribution of the projected needle area per unit ground area for individual trees as it was derived from measurements (Ellenberg et al., 1986) can be well approximated by a modified Raleigh distribution function (Constantin, 1993):

$$u_{L,z}(z) = \frac{1}{2X_C 2Y_C} \int\int u_L(x,y,z)\,\mathrm{d}x\,\mathrm{d}y = \frac{L}{a} z_r^2 \exp(-\alpha z_r),\ z_r = \frac{z}{l_z},\ z \le l_z, \tag{15}$$

where L is the leaf area index of our sample stand; a is a normalisation factor (in m) derived from averaging the variation in the vertical leaf area distribution of individual trees; α is the dimensionless parameter determining

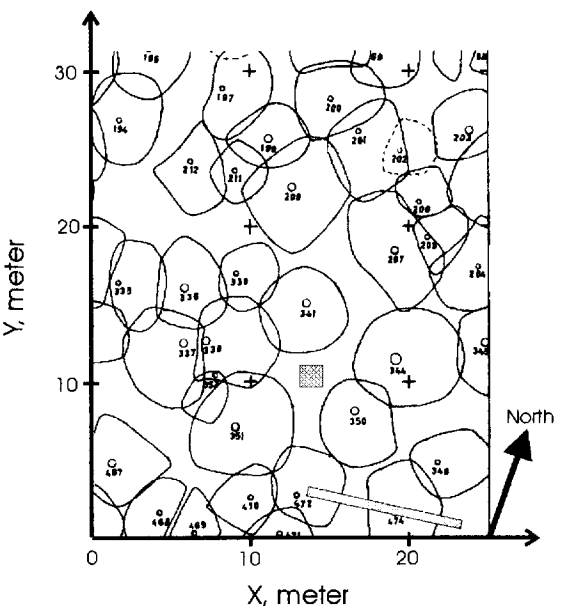

Fig. 1. Spatial distribution of crown projections in the sample spruce stand. The coordinate system is aligned such that the angle between the positive X axis and the direction to the north is 75°. Tree stems are numbered. The location of the 50 m-tall tower and the sensor's pathway are shown as shaded square and elongated rectangle. The cross symbols denote the vertexes of 10×10-m grids.

the shape of the curve (Eq. (15)) (Constantin, 1993) and l_z is the height of the tree crown. The integration in Eq. (15) is performed over the horizontal plane at the depth z.

We replace the crown projection of each individual tree by a rectangle of minimal dimension $2X_C$ and $2Y_C$ with its centre at (X_0, Y_0, Z_S), which covers the crown projection. The sides of these rectangles are parallel to the X and Y axes. The point (X_0, Y_0, Z_S) is taken as the tree trunk coordinate, and $2X_C$ and $2Y_C$ are the length and the width of the tree crown, respectively. We approximate the horizontal distribution of foliage elements in the tree crown by the quadratic expression along the X and Y coordinates (Ross, 1981; Myneni, 1991):

$$u_{L,x}(x) = 1.5\left(1 - \frac{(x - X_0)^2}{X_C^2}\right), \quad |x - X_0| \le X_C,$$

$$u_{L,y}(y) = 1.5\left(1 - \frac{(y - Y_0)^2}{Y_C^2}\right), \quad |y - Y_0| \le Y_C,$$

Thus, given the tree trunk distribution, (X_0, Y_0, Z_S), as well as the dimension of trees, $(2X_C, 2Y_C)$, it is possible to simulate the leaf area density function by

$$u_L(x,y,z) = \frac{2.25L}{a}\left(1 - \frac{(x - X_0)^2}{X_C^2}\right)\left(1 - \frac{(y - Y_0)^2}{Y_C^2}\right) z_r^2 \exp(-\alpha z_r) \tag{16}$$

if $|x - X_0| < X_C$, $|y - Y_0| < Y_C$, $0 < z < l_z$, and by $u_L(x,y,z) = 0$ otherwise.

We impose a fine spatial mesh (Eq. (14)) of a resolution A on the sample stand and the leaf area density in each of the fine cells is evaluated by averaging the leaf area density function (Eq. (16)) over the fine cell. The leaf area density of a domain obtained due to intersection of trees is the sum of the leaf area densities of the intersecting trees. As a result of this discretization, we have approximated the leaf area density function (Eq. (16)) by a piecewise constant function $u_L(A; x, y, z)$ with respect to the spatial variable $\boldsymbol{r} = (x, y, z)$ that is input for the transport equation. The accuracy of this approximation depends on the resolution A: the larger A, the

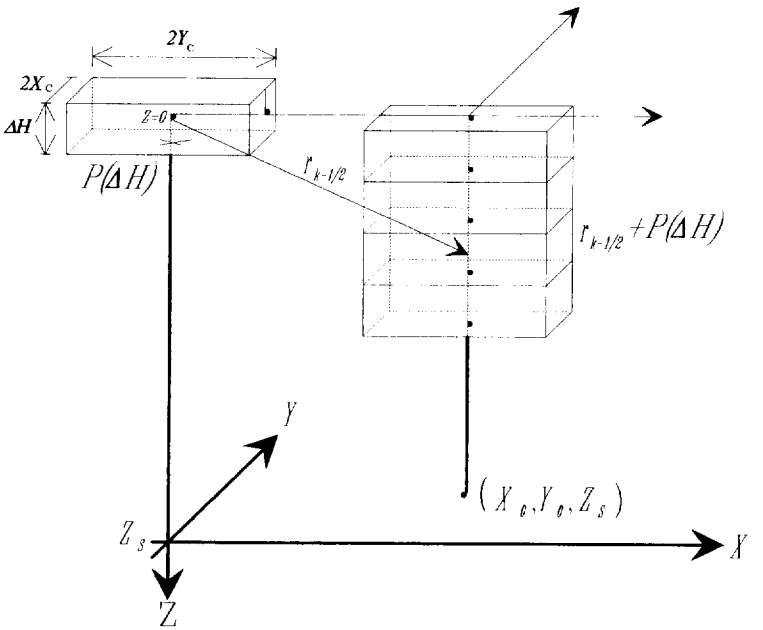

Fig. 2. Schematic representation of tree canopies. The tree crown is covered by parallelepipeds of dimension $2X_C$, $2Y_C$ and ΔH, which are obtained by shifting the parallelogram $P(\Delta H)$ along the vector $r_{k-1/2}$.

more accurate $u_L(A;x,y,z)$ approximates Eq. (16). The leaf area density function (Eq. (16)), however, simulates the forest structure with a certain degree of accuracy.

Before examining the quality of the leaf area density function $u_L(A;x,y,z)$, let us analyse as to how the vertical distribution of leaf area (Eq. (15)) for an individual tree was derived from measurements. An ideal experiment may be as follows. One splits the tree crown into horizontal layers by planes $z_k = k\Delta H$, $k = 0,1,2,\ldots,M_z$, $\Delta H = l_z/M_z$ (Fig. 2) and then bounds it vertically by the planes $x = X_0 \mp X_C$, $y = Y_0 \mp Y_C$. As a result, the tree crown is enclosed by the parallelepipeds of dimension $2X_C$, $2Y_C$ and ΔH. Evaluating the amount of foliage area in every parallelepiped, one obtains a histogram of the vertical density distribution of leaf area per unit ground area as:

$$\bar{u}_{L,z}(z) = \frac{S_k}{\Delta H 2X_C 2Y_C}, (k-1)\Delta H \le z < k\Delta H, k = 1,2,\ldots,M_z \tag{17}$$

where S_k is the area of foliage elements in the parallelepiped $\boldsymbol{r}_{k-1/2} + P(\Delta H)$; $\boldsymbol{r}_{k-1/2} = (X_0, Y_0, z_{k-1/2})$; $z_{k-1/2} = k\Delta H - \Delta H/2$ and $P(\Delta H)$ is a parallelepiped of dimension $2X_C$, $2Y_C$ and ΔH, i.e., $P(\Delta H) = \{(x,y,z) : |x| < X_C, |y| < Y_C, |z| < \Delta H/2\}$. The histogram (Eq. (17)) is then approximated by the Raleigh distribution function (Eq. (15)) (Constantin, 1993).

In the above analyses, the parallelepiped, $P(\Delta H)$, has the following property: the leaf area in a fine cell, $u_L(A;x,y,z)\Delta x\Delta y\Delta z$, can greatly differ from the real one; the mean leaf area over $P(\Delta H)$, however, coincides with the real value within an accuracy provided by the measurements. Therefore, our leaf area density function, $u_L(A;x,y,z)$, has P quality and its accuracy can be characterised by the P-volume accuracy. Here P is a parallelepiped whose faces are parallel to the XY, YZ and XZ planes. It may be shown that the solution of Eq. (10) maintains the P-quality and its P-volume accuracy cannot be better than the P-volume accuracy of the input data. A strict mathematical argument of this is a topic of a special investigation, involving the technique of functional analysis; therefore, we shall leave it for a detailed analysis at a later time [1].

3.2. Model resolution

We evaluate an appropriate resolution from the following experiment. We calculate the mean energy flux over a parallelepiped, P, as a function of the resolution, A, by using the radiation model, then compare the values of this function with the mean measured flux averaged over the same parallelepiped. Thus, we can find a resolution that provides a minimal disagreement between simulated and measured fluxes. This resolution will be taken as the model resolution needed for simulating the radiative field in our sample stand.

The sample stand described above was chosen to realise our experiment. The length l_z, of the tree crown is suggested to be constant in our calculation: $l_z = 11$ m. The leaf area index, $L = 7.4$ (Ibrom, 1993). Parameters a and α in Eq. (15) were 0.15 and 5.7, respectively. The leaf normal distribution was given by a spherical distribution in all our calculations, i.e., $g_L(\boldsymbol{r},\boldsymbol{\Omega}) = 1$. Models for simulating the boundary conditions and optical properties of the soil and the leaves as they will be described in the next sections are used in our calculations.

A moving LICOR quantum sensor that measures the quanta between 400–700 nm was installed 2 m above the ground on a horizontal support. The 10-m path of the sensor is shown in Fig. 1. The downward PAR flux (in μmol m^{-2} s^{-1}) was measured by this moving sensor so that the mean 1-h measured flux corresponds to the mean flux averaged over the sensor's path and 1-h time interval. In addition, four sensors were mounted 10 m above our forest canopy at the height of 39 m to measure incident global (diffuse plus direct) PAR (in μmol m^{-2} s^{-1}), diffuse and global (diffuse plus direct) short-wave fluxes (in W m^{-2}), as well as PAR-radiation (in

[1] The P-quality and the P-volume accuracy can be described in terms of the theory of functional analysis. Really, introducing the metric by $\|f\|_P = \sup_r(\int_{r+P}|f(r')|dr')$ we generate the Banach space of functions which have the P-quality. Mathematical investigations of the transport equation start usually with establishing the following fact: if input variables belong to a Banach space then the solution of the transport equation is also an element of the same Banach space (Vladimirov, 1963; Germogenova, 1986; Ross et al., 1992; Vainikko, 1993). It means that the solution of the transport equation maintains the quality of input data.

μmol m^{-2} s^{-1}) reflected by the forest. The measured incident radiation fluxes serve as the input for model calculation (see Section 5). An overcast sky (3 October 1994) was chosen to carry out the experiment.

According to our calculations (some of them will be presented in Section 3.3), the sensor's path can be taken as representative for the site,

$$S_R = \{(x,y): |x-12| \le 7\,\mathrm{m}, |y-14.5| \le 9.5\,\mathrm{m}\},$$

covering an area of 14×19 m^2 around the point $\boldsymbol{r} = (12\ \mathrm{m}, 14.5\ \mathrm{m}, 27\ \mathrm{m})$. Therefore, the parallelepiped, $P(\Delta z) = \{(x,y,z): |x| \le 7\ \mathrm{m}, |y| \le 9.5\ \mathrm{m}, |z| \le \Delta z/2\}$, of dimension $14 \times 19 \times \Delta z$ was chosen to specify the model resolution. Its height, Δz, is a variable in our calculation and is equal to the height of the fine cell. Because the solution of the transport equation was assumed to be constant within a fine cell, the mean radiation intensity over $P(\Delta z)$ coincides with the mean radiation intensity over a horizontal surface of area 14×19 m^2. A diurnal variation with 1-h time step of mean downward flux over the surface S_R about the point $\boldsymbol{r} = (12\ \mathrm{m}, 14.5\ \mathrm{m}, 27\ \mathrm{m})$ as a function of the model resolution, A, was calculated by using our model as:

$$M_S(A,t) = \frac{1}{v(P(\Delta z))} \int_{P(\Delta z)} d\boldsymbol{r} \int_{400\,\mathrm{nm}}^{700\,\mathrm{nm}} d\lambda \int_{2\pi^+} d\Omega I_\lambda(A,t;\boldsymbol{r},\boldsymbol{\Omega}) |\boldsymbol{\Omega} \cdot n|. \tag{18}$$

Here $v(P(\Delta z))$ denotes the volume of $P(\Delta z)$; $I_\lambda(A,t;\boldsymbol{r},\boldsymbol{\Omega})$ is the radiation intensity at a time t and corresponding the resolution, A; n is the normal to a horizontal surface.

Fig. 3 shows the dependence of the simulated mean diurnal variation, $M_S(A,t)$ on the model resolution A. The measured moving sensor response is plotted in this figure also. To characterise the difference between measured and simulated results, we use the following function of resolution A:

$$\Delta(A) = 100\% \times \frac{\int_{T_1}^{T_2} |M(t) - M_S(A,t)| dt}{\int_{T_1}^{T_2} M(t) dt} \tag{19}$$

where T_1 and T_2 are the time of the sunrise and sunset, respectively; $M(t)$ is the measured value of the moving sensor response averaged over a 1-h time interval and the sensor's path way. This function took on the following values in calculations presented in Fig. 3: $\delta(1) = 50.6\%$; $\delta(4) = 44.2\%$; $\delta(8) = 20.5\%$. The model resolution of 8 fine-cells/m^3 will be used in all our calculation presented in this paper.

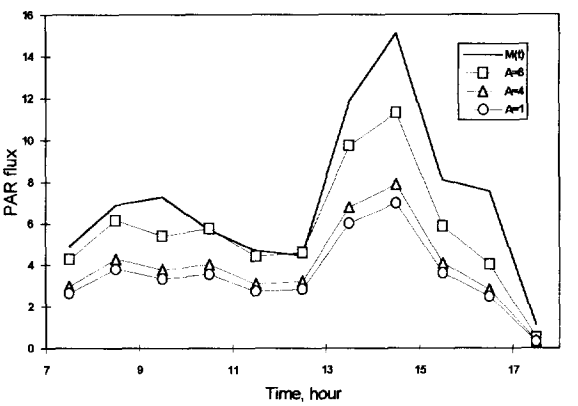

Fig. 3. Measured (legend 'M(t)') and simulated diurnal variations of mean downward fluxes (in μmol m^{-2} s^{-1}) averaged over the surface S_R (Eq. (17)) about the point $r = (12\ \mathrm{m}, 14.5\ \mathrm{m}, 27\ \mathrm{m})$ for different values of the model resolution: $A = 1/(1 \times 1 \times 1) = 1$, $1/(0.5 \times 0.5 \times 1) = 4$ and $1/(0.5 \times 0.5 \times 0.5) = 8$.

3.3. Model accuracy

Let us consider parallelepipeds $P_{14,i}(\Delta z) = S_{14,i} \times \Delta z$ and $P_{12,i}(\Delta z) = S_{12,i} \times \Delta z$ $(i = 1,2,3)$, of the height $\Delta z = 0.5$ m and with bases: $S_{14,i} = \{(x,y)$: $14 \le x \le 24$; $i \le y \le (i+1)\}$, $i = 1,2,3$; $S_{12,i} = \{(x,y)$: $12 \le x \le 22$; $i \le y \le (i+1)\}$, $i = 1,2,3$.

The area of each surface is 10 m^2. To describe the model accuracy, we examine the space variations of mean fluxes over these parallelepipeds. Let $M_{S,14,i}(t)$ and $M_{S,12,i}(t)$ be diurnal variations of mean downward fluxes over the surfaces $S_{14,i}$ and $S_{12,i}$ evaluated from Eq. (18) in which the parallelepiped $P(\Delta z)$ is replaced by $P_{14,i}(\Delta z)$ and $P_{12,i}$ correspondingly.

Fig. 4 demonstrates the behaviour of $M_{S,14,i}(t)$ and $M_{S,12,i}(t)$ as well as of $M_S(A,t)$ for a cloudy day (3 October 1994). The variations in these fluxes are caused by a variation of a surface covering an area 10 m^2 in space about the sensor's path way. The curve $M_{S,14,2}(t)$ is closest to the measured value of the moving sensor response, $M(t)$, and the surface $S_{14,2}$ is closest to the sensor's path. It allows us to suggest that 8 fine cells/m^3 are needed to simulate the diurnal variation of mean PAR fluxes over horizontal surfaces of the size about 10 m^2 with the accuracy of about 80%. The behaviour of $M_{S,14,2}(t)$ and of the sensor response, $M(t)$, during the clear sky plotted in Fig. 5 may also serve as an argument to confirm this suggestion ($\delta(8) = 18.2\%$ in this case). Comparing $M_{S,14,2}(t)$, $M_{S,14,3}(t)$ and $M(A,t)$, one can conclude that the sensor's path way may be taken as representative for the whole site, S_R.

Thus, our leaf area distribution function has 'parallelepiped' quality. The base of the parallelepiped is parallel to the XY plane. A solution of the transport equation maintains the quality of input data, i.e., the mean flux over the parallelepiped can provide an acceptable accuracy only. If its height tends to zero, the parallelepiped degenerates into a horizontal surface. This property highlights a range of applications of such models—the evaluation of mean radiation intensities over horizontal surfaces. Remote sensing problems, for example, require such an information to interpret the radiation field reflected by vegetation canopies. In photosynthesis research, this quality of input data, however, may lead to a false quantification of this process. The canopy photosynthesis results from the interaction between the photosynthetic response of foliage elements and the radiation incident at these elements. Therefore, input data must possess more various qualities in order to estimate the radiation fluxes over the surfaces of different inclinations correctly.

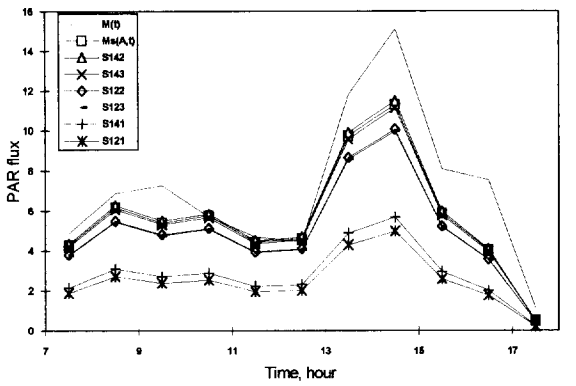

Fig. 4. Diurnal variation of mean downward fluxes (in μmol m^{-2} s^{-1}) averaged over different surfaces, $S_{12,i}$ (legend 'S12i') and $S_{14,i}$ (legend 'S14i'), $i = 1, 2, 3$, of an area 10 m^2. The sensor response (legend 'M(t)') and the mean downward flux over the surface S_R (legend '$M_S(A,t)$') are plotted also.

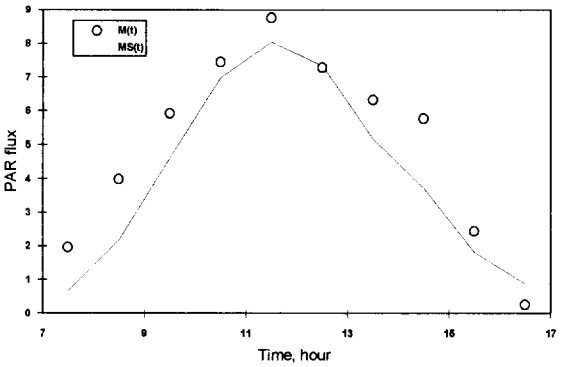

Fig. 5. Measured (legend '$M(t)$') and modelled (legend '$Ms(t)$') diurnal variations of mean downward fluxes (in μmol m^{-2} s^{-1}) averaged over the surface S_R on a clear sunny day (15 October 1994).

3.4. Basic foliage element

Fine spatial cells introduced by Eq. (14) are considered the elementary volumes in our model. Different cells may have different properties that are mean values of scattering and geometrical properties of chosen foliage elements in the cell. Their specification, therefore, depends on which foliage elements are referred to. A coniferous one-year shoot of size 5–7 cm with needles was taken as the basic foliage element in the present paper. In Section 6 we will discuss the spectral reflection and transmittance of our basic foliage element. In addition, a description of their geometrical properties is required to quantify the optical property (the total interaction and differential scattering cross-sections) of an elementary volume. The leaf area density function is used to parameterize the foliage geometry in our approach. Its value depends on how the 'area of the one-year shoot' is determined. The projected needle area (Smolander et al., 1994) has commonly been considered to quantify a one-side area of nonflat leaves (needles). Although the one-year shoot was taken as the basic foliage element and its optical properties are the basis of our simulation, the meaning of the one-year shoot area has not been clarified by the above discussions. Really, parameters for the modified Raleigh distribution function (Eq. (15)) were derived by averaging the vertical distribution of total needle area of individual trees (Constantin, 1993). It may dilute shoot architecture properties. The constant ratio, $S = 2.74$, between total and projected needle area (Riederer et al., 1988) was then used in our model to convert the distribution of total needle area to the projected one. This ratio, however, may vary within tree crowns. Our model of the leaf scattering phase function (see Section 4) does not account for the shoot architecture (Ross et al., 1994). Thus, we cannot assert that the total interaction and differential scattering cross-sections were derived from our basic foliage element.

As a result of the discretization, the leaf area density function, $u_L(x,y,z)$ (Eq. (16)) was replaced by a piecewise constant function, $u(A,x,y,z)$ which then was used in our calculations. This function depends now on A, and is equal to the original one only if A tends to infinity, i.e., $u_L(\infty;x,y,z) = u_L(x,y,z)$. By varying A, it is possible to change the leaf area density function in a certain range. We specify the model resolution by solving the following inverse problem: find A for which the difference, $\delta(A)$ (Eq. (19)), between measured and simulated results takes on a minimal value. In spite of the uncertainty in defining a one-year shoot area, it is, therefore, possible to use the function $u_L(A,x,y,z)$ for modelling the leaf area distribution by choosing an appropriate model resolution. The model resolution depends, in its turn, on an overall accuracy of all input data. The effect of the model resolution on the leaf area density function can be seen, for example, when we evaluate the leaf area indexes for our sample stand, LAI and LAI_A, evaluated from $u_L(x,y,z)$ and $u_L(A,x,y,z)$: LAI = 6.06; $\mathrm{LAI}_A = 5.57$ ($A = 8$). Note that such an approach is widely used in numerical solution of ill-posed problems (Tikhonov and Arsenin, 1979). This technique, however, may lead to systematic errors that were observed in our calculations.

4. Optical properties of the foliage

We distinguish two types of scattering: a photon can either be specularly reflected at the surface of the foliage element or can undergo multiple interactions inside the foliage element before leaving it. Therefore, the leaf scattering phase function, $\gamma_{L,\lambda}(\boldsymbol{r},\boldsymbol{\Omega}_L,\boldsymbol{\Omega}'\rightarrow\boldsymbol{\Omega})$, consists of two parts, the specular and the diffuse contributions (Myneni, 1991; Knyazikhin and Marshak, 1991; Myneni et al., 1991):

$$\gamma_{L,\lambda}(\boldsymbol{r},\boldsymbol{\Omega}_L,\boldsymbol{\Omega}'\rightarrow\boldsymbol{\Omega}) = \gamma_S(\boldsymbol{r},\boldsymbol{\Omega}_L,\boldsymbol{\Omega}'\rightarrow\boldsymbol{\Omega}) + \gamma_{D,\lambda}(\boldsymbol{r},\boldsymbol{\Omega}_L,\boldsymbol{\Omega}'\rightarrow\boldsymbol{\Omega})$$

The specular reflection is supposed to be independent on wavelength. A model for the specular reflection proposed by Vanderbilt and Grant (1985) is incorporated into our model:

$$\gamma_S(\boldsymbol{r},\boldsymbol{\Omega}_L,\boldsymbol{\Omega}'\rightarrow\boldsymbol{\Omega}) = K(\kappa,\alpha')F(\nu,\alpha)\delta(\boldsymbol{\Omega}\cdot\boldsymbol{\Omega}^*)$$

where α' is the angle between the incident ray $\boldsymbol{\Omega}'$, and the leaf normal $\boldsymbol{\Omega}_L$; $F(\nu,\alpha')$ is the Fresnel reflectance (averaged over the polarisation states); $K(\kappa,\alpha')$ defines the correction factor for specular reflection; n is the wax refraction index; κ is the smoothness of the leaf surface and $\boldsymbol{\Omega}^*$ is the direction of specular reflection. The correction factor, $K(\kappa,\alpha') = \exp(-\kappa\ \tan|\alpha'|)$, proposed by Ross et al. (1992) was used in our calculations. Parameters κ and ν were 0 and 1.5, respectively. For more details of these results, the reader may consult Myneni (1991), Myneni et al. (1991) and Ross et al. (1992).

The leaf scattering phase function for the diffuse distribution is supposed bi-Lambertian (Ross and Nilson, 1968), i.e., a fraction of the energy intercepted by the foliage element may be reflected or transmitted in a cosine distribution about the leaf normal, i.e.,

$$\gamma_{D,\lambda}(\boldsymbol{r},\boldsymbol{\Omega}_L,\boldsymbol{\Omega}'\rightarrow\boldsymbol{\Omega}) = \begin{cases} \pi^{-1}r_{D,\lambda}(\boldsymbol{r})|\boldsymbol{\Omega}\cdot\boldsymbol{\Omega}_L|, & (\boldsymbol{\Omega}\cdot\boldsymbol{\Omega}_L)(\boldsymbol{\Omega}'\cdot\boldsymbol{\Omega}_L)<0, \\ \pi^{-1}t_{D,\lambda}(\boldsymbol{r})|\boldsymbol{\Omega}\cdot\boldsymbol{\Omega}_L|, & (\boldsymbol{\Omega}\cdot\boldsymbol{\Omega}_L)(\boldsymbol{\Omega}'\cdot\boldsymbol{\Omega}_L)>0 \end{cases}.$$

Here $r_{D,\lambda}$ and $t_{D,\lambda}$ are the spectral reflection and the spectral transmittance of the leaf element, and they depend on wavelength. We define the spectral scattering coefficient, $d_\lambda(\boldsymbol{r})$, as

$$d_\lambda(\boldsymbol{r}) = \int_{4\pi}\gamma_{D,\lambda}(\boldsymbol{r},\boldsymbol{\Omega}_L,\boldsymbol{\Omega}'\rightarrow\boldsymbol{\Omega})\mathrm{d}\boldsymbol{\Omega},$$

that is a fraction of the intercepted energy diffusely reflected by the one-year shoot. This variable influences in a high degree the radiative regime in the vegetation. It may be shown that $d_\lambda(\boldsymbol{r}) = r_{D,\lambda}(\boldsymbol{r}) + t_{D,\lambda}(\boldsymbol{r})$ (Knyazikhin and Marshak, 1991).

A measurement programme accompanied our model development to derive a spatial distribution of $r_{D,\lambda}(\boldsymbol{r})$ and $t_{D,\lambda}(\boldsymbol{r})$. A coniferous one-year shoot of size 5–7 cm was considered the basic foliage element. Three characteristics of the one-year shoot were chosen to experimentally examine the spatial variation of foliage spectral properties. These are (1) age of needles on the one-year shoot; (2) position within the tree crown (upper, two middle and lower parts) and (3) geographical orientation with respect to the tree stem (south, north, east and west). The LI-1800/22 portable spectroradiometer with the external integrating sphere (LI-1800-12 S) device was used to measure the spectral reflection and transmittance of one-year shoots in the region from 300 to 1100 nm with the spectral step of 1 nm. Our experiment was carried out in September, i.e., at the end of the vegetation season, when the needles of the current year are already formed. Fig. 6 shows an example of the sensitivity of the one-year shoot spectral reflection to each of these chosen attributes. One can see that the optical properties of these one-year shoots depend both on wavelength and the one-year shoot position in space. The spectral scattering coefficient, $d_\lambda(\boldsymbol{r})$, varies from its mean value over the spectral range and over the one-year shoot attributes, on the average, by 33%. If, however, we compare the spectral scattering coefficients with its mean spectral variations taken over one-year shoot attributes, then the deviation is, on the average, 12% only, not exceeding our measurement mistake in the spectral transmittance. Therefore, the mean of the one-year shoot spectral transmittance coefficient and the mean reflection coefficient averaged over all one-year shoot

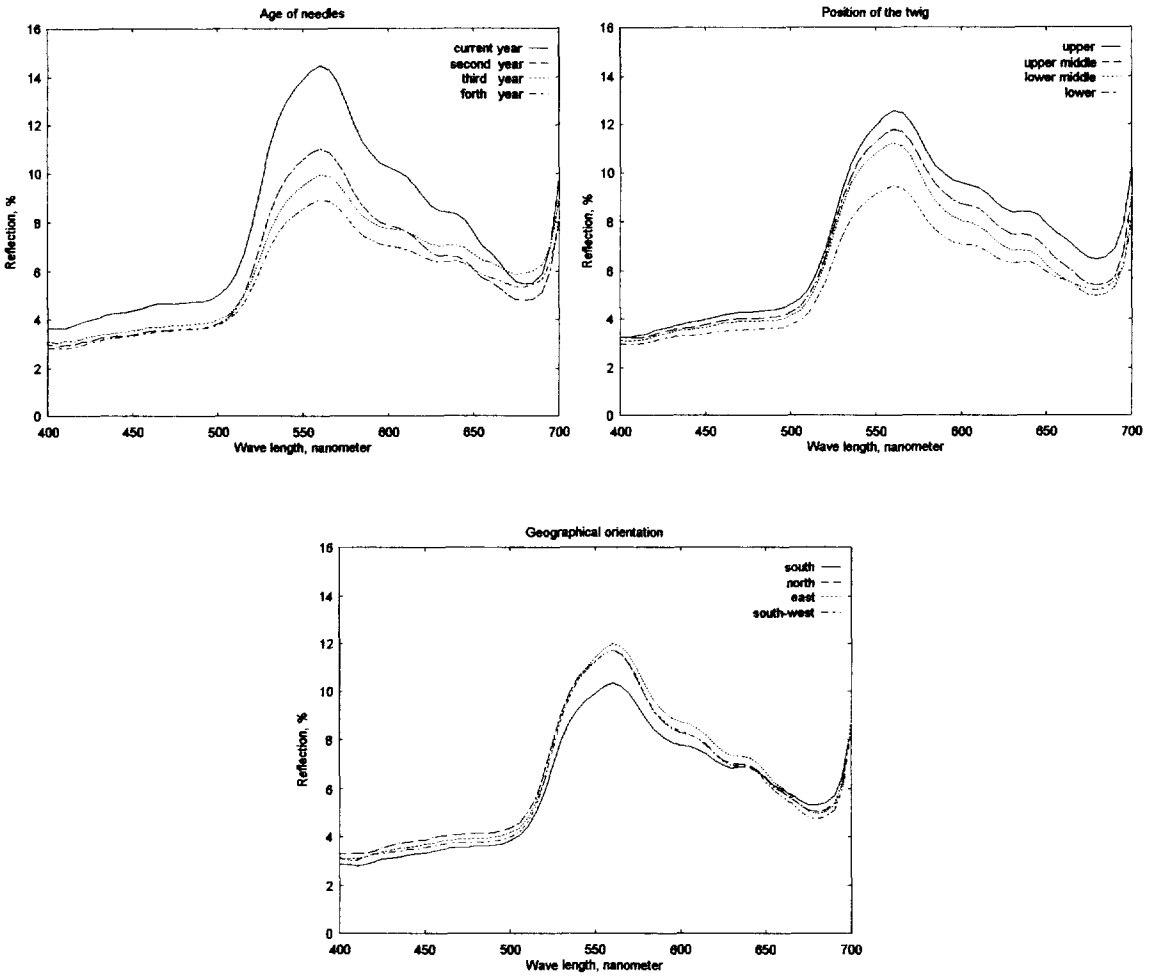

Fig. 6. The spectral reflection of spruce one-year shoots derived from measurements. Three characteristics of the one-year shoots were chosen to examine the spatial variations of foliage spectral properties, age of needles on the one-year shoot; position within the tree crown (upper, two middle and lower); and geographical orientation with respect to the tree stem (south, north, east and west). The mean reflection taken over spatial and spectral variables is 6%.

attributes introduced above were taken as $r_{D,\lambda}$ and $t_{D,\lambda}$ in our calculations, i.e., we ignore in our calculations the spatial variation of foliage optical properties but consider its spectral variation.

5. Boundary conditions

The solar radiation penetrating through the canopy boundary, δV, determine the radiative field in a forest canopy. The boundary conditions for a three-dimensional canopy are also three-dimensional: the incoming radiation at the top (atmospheric, δV_t) and at the bottom (soil, δV_b), as well as at the lateral (neighbouring canopy, δV_l) surfaces are different. The spectral composition of the incoming radiation also influences the radiative regime in a forest canopy: photons having different wavelength interact with phytoelements differently (Section 4). The aim of this section is to simulate the spatial, spectral and angular distribution of the incoming

solar radiation, also to parameterize them in terms of the radiance energy received by a horizontal unit surface above the forest canopy—diffuse and global short-wave radiation, and global PAR radiation, which are usually known from radiation measurements.

5.1. Input variables and separation of direct beam of solar radiation

We denote by R_p, R_d and R_s the energy fluxes per horizontal surface above the forest canopy of the global PAR, diffuse short-wave and global short-wave radiation. In terms of the notations introduced by Eqs. (5) and (6) these variables may be expressed as:

$$\begin{aligned} R_p &= \int_{400\,nm}^{700\,nm} d\lambda \int_{2\pi^+} \left[T_{d,\lambda}(\boldsymbol{r}_t, \boldsymbol{\Omega}) + T_{m,\lambda}(\boldsymbol{r}_t)\,\delta(\boldsymbol{\Omega} - \boldsymbol{\Omega}_0) \right] |\boldsymbol{\Omega} \cdot n_t| d\boldsymbol{\Omega} = R_{p,d} + R_{p,m}, \\ R_d &= \int_{0\,nm}^{3000\,nm} d\lambda \int_{2\pi^+} T_{d,\lambda}(\boldsymbol{r}, \boldsymbol{\Omega}) |\boldsymbol{\Omega} \cdot n_t| d\boldsymbol{\Omega}, \\ R_s &= \int_{0\,nm}^{3000\,nm} d\lambda \int_{2\pi^+} \left[T_{d,\lambda}(\boldsymbol{r}_t, \boldsymbol{\Omega}) + T_{m,\lambda}(\boldsymbol{r}_t)\,\delta(\boldsymbol{\Omega} - \boldsymbol{\Omega}_0) \right] |\boldsymbol{\Omega} \cdot n_t| d\boldsymbol{\Omega}, \end{aligned} \tag{20}$$

where n_t is the outward normal at point $\boldsymbol{r}_t \in \delta V_t$; $R_{p,d}$ and $R_{p,m}$ are PAR fluxes generated by the diffuse and the monodirectional components of solar radiation, i.e.,

$$\begin{aligned} R_{p,d} &= \int_{300\,nm}^{700\,nm} d\lambda \int_{2\pi^+} T_{d,\lambda}(\boldsymbol{r}_t, \boldsymbol{\Omega}) |\boldsymbol{\Omega} \cdot n_t| d\boldsymbol{\Omega}, \\ R_{p,m} &= \int_{400\,nm}^{700\,nm} d\lambda \int_{2\pi^+} T_{m,\lambda}(\boldsymbol{r}_t)\,\delta(\boldsymbol{\Omega} - \boldsymbol{\Omega}_0) |\boldsymbol{\Omega} \cdot n_t| d\boldsymbol{\Omega} = |\mu_0| \int_{400\,nm}^{700\,nm} T_{m,\lambda}(\boldsymbol{r}) d\lambda. \end{aligned} \tag{21}$$

We assume that R_p, R_d and R_s do not depend on $\boldsymbol{r}_t \in \delta V_t$ at a given instant of time. Because we simulate the radiative field in a forest canopy of a small area, this suggestion is realistic even in a case when the incoming radiation is influenced by broken clouds. Three sensors were mounted 10 m above our sample stand at the height 39 m to continuously measure R_p, R_d and R_s. These variables are inputs for our model.

From our description of the radiation transport (Eqs. (8)–(13)) it follows that we require $T_{d,\lambda}(\boldsymbol{\Omega})$ and $T_{m,\lambda}(\boldsymbol{r})$ to specify the radiation incident at the top surface of the canopy. The problem now is to deduce this information from R_p, R_d and R_s. We start with separating $R_{p,m}$, and $R_{p,d}$ from the total PAR flux, using the following result (Spitters et al., 1986): the ratio between the incident diffuse and global PAR fluxes is 1.4 times larger than the same ratio for the short-wave solar radiation, i.e., $R_{p,d}/R_p = 1.4(R_d/R_s)$. Thus, given a known energy flux per horizontal surface above the forest canopy of the global PAR, the diffuse short-wave and the global short-wave radiation, it is possible to separate the incident as direct, $R_{p,m}$, and diffuse, $R_{p,d}$, fluxes from the global PAR irradiance, R_p:

$$\begin{aligned} R_{p,d} &= 1.4 \frac{R_d}{R_s} R_p, \\ R_{p,m} &= R_p - R_{p,d} = \left(1 - 1.4 \frac{R_d}{R_s} \right) R_p. \end{aligned}$$

5.2. Spectral composition of the incoming radiation

The spectral composition of solar radiation at the earth's surface depends on the atmospheric conditions and may vary largely throughout the day. These variations are mainly influenced by the sun's path, by atmospheric transparency conditions, and by clouds. In spite of these variations, however, normalised energy distribution curves of the direct solar beam in the visible region at the earth's surface corresponding to various atmospheric

conditions and the solar zenith distances were found to be close to a normalised curve of the blackbody emission spectrum at $T = 5200$ K (Kondratyev, 1969, p. 230). A radiant flux value at $\lambda = 560$ nm can be used as a normalisation factor (Kondratyev, 1969, p. 230). This assumption is used in our approach to deduce the spectral composition, $T_{m,\lambda}(\boldsymbol{r}_t)$, from the direct PAR beam.

Let $E_\lambda(T)$ be the Planck function. The probability density, $p(\lambda)$, that a photon in the direct solar radiation at the earth's surface falls in a spectral interval $(\lambda, \lambda + d\lambda)$, can be expressed as:

$$p(\lambda) = \frac{E_\lambda(5200\ \mathrm{K})}{\int_{400\ \mathrm{nm}}^{700\ \mathrm{nm}} E_\lambda(5200\ \mathrm{K})}.$$

Thus, given a known the total flux of photons, $R_{p,m}$ (in μmol m^{-2} s^{-1}), it is possible to evaluate the spectral composition of the direct solar beam as $T_{m,\lambda}(\boldsymbol{r}_t) = p(\lambda)\ R_{p,m}$.

As it was mentioned in Section 2 the radiation intensity, $I_\lambda(\boldsymbol{r}, \boldsymbol{\Omega})$ can be expressed via the sum of the direct, $I_{m,\lambda}(\boldsymbol{r}, \boldsymbol{\Omega})$, and the diffuse, $I_{d,\lambda}(\boldsymbol{r}, \boldsymbol{\Omega})$, radiation intensities. The second addend, in its turn, can also be represented by the sum of two components, viz.

$$I_{d,\lambda}(\boldsymbol{r}, \boldsymbol{\Omega}) = I^1_{d,\lambda}(\boldsymbol{r}, \boldsymbol{\Omega}) + I^2_{d,\lambda}(\boldsymbol{r}, \boldsymbol{\Omega}). \tag{22}$$

The first component is the radiation intensity results from interaction of the incoming diffuse radiation with the forest canopy. It satisfies Eqs. (10)–(13) in which $Q_{0,\lambda}(\boldsymbol{r}) = 0$ and $\rho_{\lambda,l} = \rho_{\lambda,b} = 0$. The second component, $I^2_{d,\lambda}(\boldsymbol{r}, \boldsymbol{\Omega})$, describes the rest radiative field. It satisfies an equation obtained from substituting Eq. (22) in Eqs. (10)–(13).

$I^1_{d,\lambda}(\boldsymbol{r}, \boldsymbol{\Omega})$ depends on the diffuse radiation only. In the photosynthetically active region of the solar spectrum, leaves are usually absorbed 85–90% of intercepted radiation. A contribution of the multiscattered photons to the radiative field makes up 10–15% (Knyazikhin and Marshak, 1991). Thus, neglecting multiplied scattered photons does not reduce the accuracy of our calculations. Therefore, $I^1_{d,\lambda}(\boldsymbol{r}, \boldsymbol{\Omega})$ can be approximated reasonably well by single scattering radiation, $J^1_{d,\lambda}(\boldsymbol{r}, \boldsymbol{\Omega})$, i.e., $I^1_{d,\lambda}(\boldsymbol{r}, \boldsymbol{\Omega}) \approx J^1_{d,\lambda}(\boldsymbol{r}, \boldsymbol{\Omega})$. In terms of mathematical symbols it means that we ignore the integral term in Eq. (10) to specify the single scattering radiation (Ross et al., 1992), i.e., $J^1_{d,\lambda}(\boldsymbol{r}, \boldsymbol{\Omega})$ satisfies Eqs. (10)–(13) in which $\sigma_{s,\lambda} = 0$, $Q_{0,\lambda}(\boldsymbol{r}) = 0$ and $\rho_{\lambda,l} = \rho_{\lambda,b} = 0$. Integrating these equations with respect to λ over the spectral interval 400–700 nm, we obtain equations for the radiation intensity, $J_p(r, \Omega) = \int_{300\ \mathrm{nm}}^{700\ \mathrm{nm}} J^1_{d,\lambda}(\boldsymbol{r}, \boldsymbol{\Omega}) d\lambda$, of single scattered photosynthetically active radiation:

$$\begin{aligned}
&\boldsymbol{\Omega} \cdot \nabla J_p(\boldsymbol{r}, \boldsymbol{\Omega}) + \sigma(\boldsymbol{r}, \boldsymbol{\Omega}) J_p(\boldsymbol{r}, \boldsymbol{\Omega}) = 0,\\
&J_p(\boldsymbol{r}_t, \boldsymbol{\Omega}) = \int_{400\ \mathrm{nm}}^{700\ \mathrm{nm}} T_{d,\lambda}(\boldsymbol{r}_t, \boldsymbol{\Omega}) d\lambda = T_{d,p}(r_t, \boldsymbol{\Omega}),\ \boldsymbol{r}_t \in \delta V_t, \boldsymbol{\Omega} \cdot n_t < 0,\\
&J_p(\boldsymbol{r}_l, \Omega) = \int_{400\ \mathrm{nm}}^{700\ \mathrm{nm}} L_{d,\lambda}(\boldsymbol{r}_l, \Omega) d\lambda = L_{d,p}(\boldsymbol{r}_l, \boldsymbol{\Omega}),\ \boldsymbol{r}_l \in \delta V_l, \boldsymbol{\Omega} \cdot n_l < 0,\\
&J_p(\boldsymbol{r}_b, \boldsymbol{\Omega}) = 0,\ \boldsymbol{r}_b \in \delta V_b \boldsymbol{\Omega} \cdot n_b < 0
\end{aligned} \tag{23}$$

It follows from these equations that J_p depends on $T_{d,p}$ and $L_{d,p}$, the integrals over PAR spectral interval. Neglecting the spectral composition of the incoming diffuse radiation, therefore, does not exceed the accuracy of our measurements. Thus, we will ignore the spectral composition of the incoming diffuse radiation in our model.

The dependence of $I^2_{d,\lambda}$ on the wavelength cannot be ignored. This component results from the interaction of photons in the direct solar beam with phytoelements. Photons of different wavelength interact with phytoelements differently (Section 4). Therefore, the intensity of the PAR energy is a weighted sum of monochromatic radiation intensities. The weights are determined by a spectral composition of the solar beam. This makes the radiative field sensitive to spectral properties of both phytoelements and the incoming radiation. To illustrate, we simulate two vertical profiles of horizontally averaged PAR fluxes. In the first case, we account for the

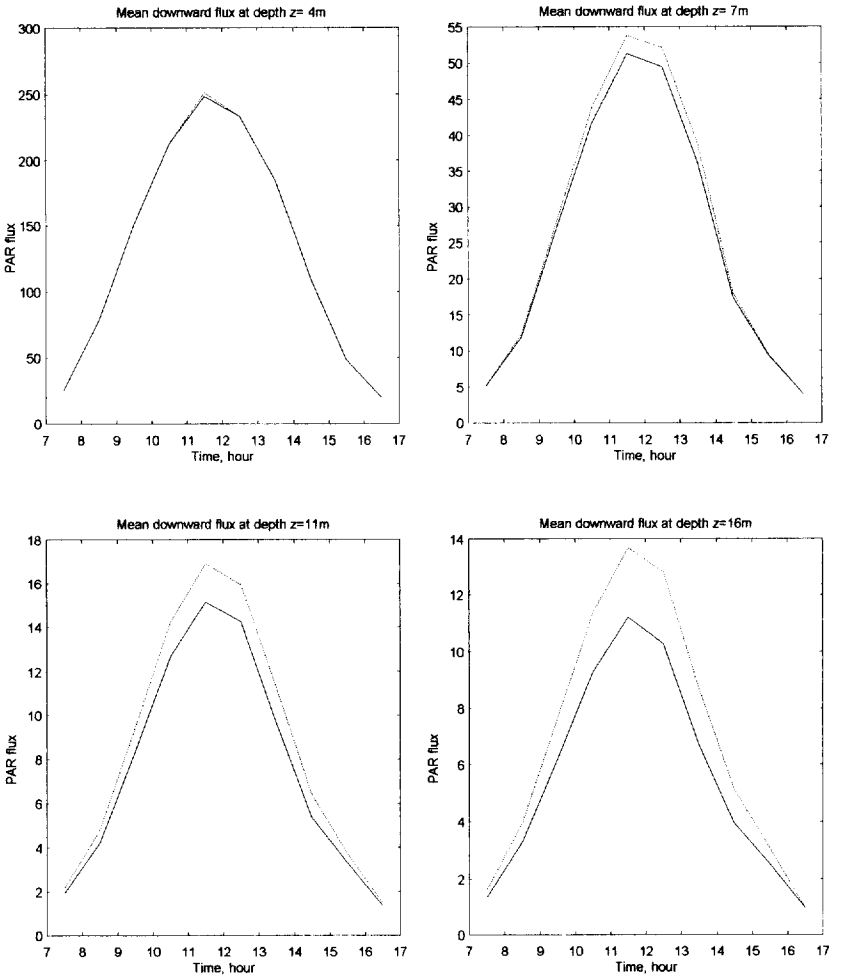

Fig. 7. Diurnal variation of horizontally averaged PAR fluxes (in μmol m^{-2} s^{-1}) at various depths below the top of the canopy at 29 m. Solid line: the spectral reflectance and transmittance of one-year shoot are considered; dotted line: the spectral reflectance and transmittance of one-year shoot are ignored.

spectral variation of one-year shoot reflectance and transmittance described in Section 4. In the second one, the reflection and transmittance coefficients are constant with respect to the wavelength and equal to their mean values over the PAR region of the solar spectrum. Diurnal variations of these horizontally mean fluxes at different depths on a clear sunny day are shown in Fig. 7. The difference between these fields defined accordingly by Eq. (19) increases with moving away from the top surface towards the soil, reaching the value of 26% under the tree crown level.

5.3. Angular distribution of the incoming diffuse radiation

Models for conditions of a standard overcast and a clear sky were incorporated in our approach to simulate the diffuse radiation, $T_{d,p}$, incident on the top surface of the canopy boundary. In the first case, the standard

overcast sky, the intensity of the incoming diffuse radiation is suggested to be independent on azimuth and approximated by:

$$T_{d,p}(\boldsymbol{r},\boldsymbol{\Omega}) = i(\pi)\frac{1+b|\cos(v)|}{1+b},\ \boldsymbol{\Omega} \sim (\mu,\phi),\vartheta = \arccos(\mu) > \frac{\pi}{2},\ \boldsymbol{r} \in \delta V_t, \tag{24}$$

where $1+b$ is the ratio between sky brightness in the zenith, $i(\pi)$, and at the horizon, $i(\pi/2)$, and it varies between 2.1 and 2.4 (Monteith and Unsworth, 1990). Substituting Eq. (23) into Eq. (21) and taking into account Eq. (24), we can express $i(\pi)$ as:

$$i(\pi) = R_{p,d}\frac{1+b}{\pi\left(1+\frac{2}{3}b\right)}$$

In the second case, a model of the clear sky proposed by Pokrowski (1929) is used to simulate the incoming diffuse radiation during sunny days:

$$T_{d,p}(\boldsymbol{r},\boldsymbol{\Omega}) = i_0\left(1-\exp\left(\frac{-0.32}{|\mu|}\right)\right)\frac{1+\boldsymbol{\Omega}\cdot\boldsymbol{\Omega}_0}{1-\boldsymbol{\Omega}\cdot\boldsymbol{\Omega}_0},\ \boldsymbol{\Omega} \sim (\mu,\phi),\mu < 0$$

where i_0 is the sky brightness in a direction at the horizon that can be specified in the same way as above.

5.4. Radiation penetrating through lateral sides

The radiation penetrating through the lateral canopy sides strongly depends on the neighbouring environment. Its influence on the radiative field in the forest canopy is essential near the lateral canopy boundary. Inaccuracies in the lateral boundary conditions, therefore, cause essential distortions in the simulated radiative field in this domain. These distortions, however, decrease with moving away from this boundary towards the centre of the stand. When the radiative regime in a extended forest is analysed, this side effect can be neglected. Inaccuracies in the boundary conditions can, however, put problems in investigating the radiation distribution in a small canopy because the dimension of the 'distorted area' can be comparable to the dimension of the chosen site. A problem then arises as to how the inaccuracies in the boundary conditions can be minimised.

In the frame of our model, the 'predictor–corrector' technique (Hall and Watt, 1976) is realised to achieve this goal. It means we predict the radiative field in a tree sample stand by solving a one-dimensional vertical transport equation at first. Its solution, i.e., the vertical profile of the horizontally averaged radiation intensity, is taken then as the radiation penetrating through the lateral canopy boundary. The average of our three-dimensional total interaction (Eq. (2)) and differential scattering (Eq. (3)) cross-sections over horizontal surfaces provides vertical profiles of required input coefficients for the one-dimensional transport equation which, on the average, consider features of both the simulated canopy and its neighbouring environment. Information about angular distribution and spectral composition of radiation incident on the top canopy boundary is also needed to solve the one-dimensional transport equation. The models of the incoming radiation described in previous subsections serve as input to predict the radiative field. Thus, the 'predictor–corrector' technique allows us to simulate the lateral boundary conditions, accounting a complicated process of photon interactions both with the chosen forest site and with its neighbouring environment. A dependence of size of the 'distorted area' induced by utilising our approach on adjoint vegetation, on the atmospheric conditions and the model resolution was studied by Kranigk (1996). In particular, it has been shown that the 'distorted area' consists of space points being less than about 5 m apart from the lateral boundary of the forest. This area, therefore, must be excluded from the analysis.

A neighbouring environment influences the radiative regime in a forest of a small area. To demonstrate a range of this influence we simulate two extreme situations. In the first one, we cut the forest surrounding our

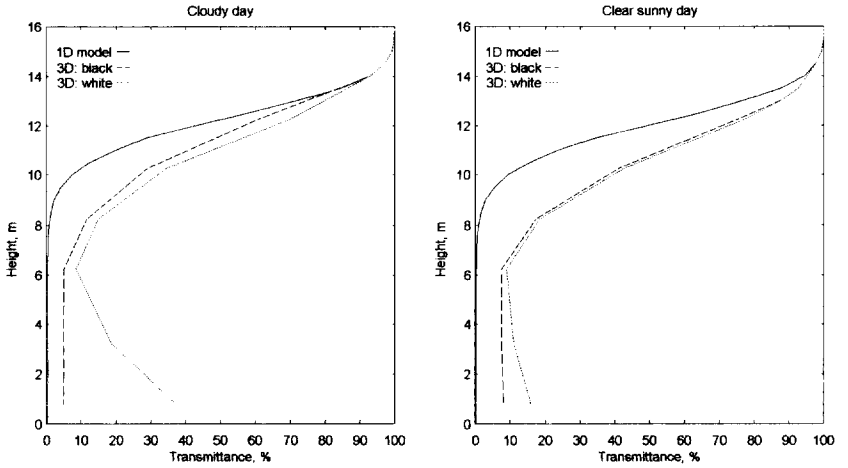

Fig. 8. Vertical profile of the canopy transmittance derived from the one-dimensional (legend '1D model') and three-dimensional (legends '3D black' and '3D white') models on a cloudy day and on a clear sunny day. Curves '3D: black' correspond to a forest stand of a small area surrounded by the optically black lateral boundary, and curves '3D: white' to an isolated forest stand of the same size and structure.

sample stand. In this case the incoming solar radiation can reach the sides of our sample stand without experiencing a collision. The lateral boundary condition (Eq. (6)) coincides with Eq. (5) in this case: $I_\lambda(\boldsymbol{r}_1, \boldsymbol{\Omega}) = L_{d,\lambda}(\boldsymbol{r}_1, \boldsymbol{\Omega}) + L_{m,\lambda}(\boldsymbol{r}_1)\ \delta(\boldsymbol{\Omega} - \boldsymbol{\Omega}_0)$, $\boldsymbol{r}_1 \in \delta V_1$, $\boldsymbol{\Omega} \cdot n_1 < 0$.

In the second situation, we 'plant' a forest of an extremely high density around our sample stand so that no solar energy can pass through the vertical boundary. The lateral boundary conditions for these optically black vertical sides are expressed as: $I_\lambda(\boldsymbol{r}_1, \boldsymbol{\Omega}) = 0$, $\boldsymbol{r}_1 \in \delta V_1$, $\boldsymbol{\Omega} \cdot n_1 < 0$.The radiative regimes in a real stand usually vary between these extreme situations. For each situation we estimate the vertical profile of the canopy transmittance, $T(z)$, as:

$$T(z) = \frac{1}{R_p} \frac{1}{m(S_R)} \int_{z+S_R} \mathrm{d}x \mathrm{d}y \int_{400\ \mathrm{nm}}^{700\ \mathrm{nm}} \mathrm{d}\lambda \int_{2\pi^+} I_\lambda(x, y, z, \boldsymbol{\Omega}) |\boldsymbol{\Omega} \cdot n| \mathrm{d}\boldsymbol{\Omega},$$

where S_R is the horizontal surface of the area $m(S_R) = 40 \times 40\ \mathrm{m}^2$ at the soil level; $z + S_R$ is the same surface but at the depth z. Fig. 8 shows these canopy transmittances at noon on a clear and on a sunny day in a sample stand Lange Bramke (Knyazikhin et al., 1996). A 'predicted' canopy transmittance evaluated from the one-dimensional transport equation is plotted in this figure also. One can see that the radiative regime in the forest of a small area is more sensitive to the lateral boundary conditions during cloudy days. The radiation transmittance in both cases, however, is quite higher than the one derived from the one-dimensional transport equation.

6. What do we know about forest albedo?

By definition, the forest solar albedo is the ratio of the total solar energy reflected by the forest to the single incident at the forest. To measure the forest albedo, two hemispherical sensors are usually mounted above the forest canopy. The first one records the downward energy flux incident at a horizontal surface above the forest and the second one, the upward energy flux reflected by the forest. The ratio between these measured fluxes is usually interpreted as the forest albedo. The aim of this section is to show that such measurement of the forest albedo does not provide a real albedo, at least when the PAR albedo is evaluated.

We consider our sample stand described in Section 3. We denote by $\boldsymbol{r}_S = (x_S, y_S, -h)$ the coordinates of the sensor located above the forest canopy at the height h (Fig. 9). Let $J_S(\boldsymbol{\Omega})$ be the radiation intensity of the PAR

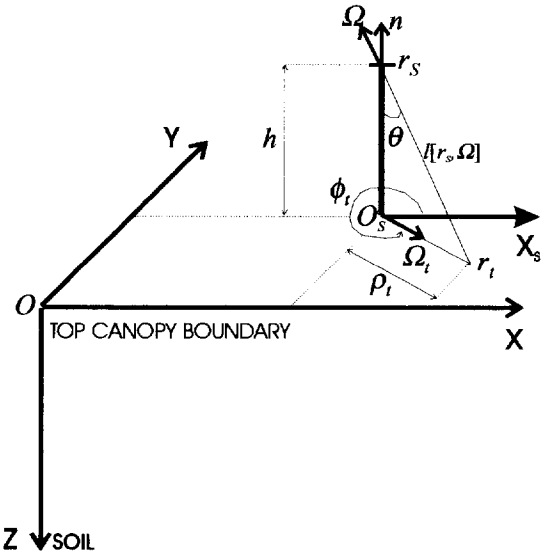

Fig. 9. Coordinate system for a downward facing sensor. Here, $\boldsymbol{r}_S$ is the point of sensor location; n is the upward normal to the sensor surface; $\boldsymbol{\Omega}$ is a direction of radiant energy captured by the sensor; $\theta = \cos^{-1}\mu$ is the angle between the direction $\boldsymbol{\Omega}$ and the normal n; $l[\boldsymbol{r}_S, \boldsymbol{\Omega}]$ is the distance between the sensor and the top canopy boundary, δV_t, along the direction $-\boldsymbol{\Omega}$; $\boldsymbol{r}_t = \boldsymbol{r}_S - l[\boldsymbol{r}_S, \boldsymbol{\Omega}]\boldsymbol{\Omega}$ is a point of the top canopy boundary; O_S is the projection of the point $\boldsymbol{r}_S$ onto the top canopy boundary. Points of the top canopy boundary are expressed in polar coordinates, ρ_t and ϕ_t, with its pole at the point O_S and polar axes $O_S X_S$ parallel to OX; $\boldsymbol{\Omega}_t$ is a unit vector at the point O_S directed to r_t.

irradiance at the point $\boldsymbol{r}_S$ in the upward direction $\boldsymbol{\Omega} \sim (\mu, \phi)$. The upward PAR energy flux reflected by the forest and captured by the sensor can be expressed as:

$$E_S = \int_{2\pi^+} J_S(\boldsymbol{\Omega}) |\boldsymbol{\Omega} \cdot n_t| \mathrm{d}\boldsymbol{\Omega} = \int_0^1 \int_0^{2\pi} J_S(\boldsymbol{\Omega}) \mu \mathrm{d}\mu \mathrm{d}\phi. \tag{25}$$

We term the ratio, A_S, of this captured energy, E_S, to the incident PAR energy, R_p (Eq. (20)), an assumed albedo, i.e.,

$$A_S = E_S / R_p. \tag{26}$$

A mean amount E_F of the PAR energy reflected by a horizontal surface S_0 of an area $m(S_0)$ in the upper crown level (i.e., $z = 0$) is:

$$E_F(S_0) = \frac{1}{m(S_0)} \int\int_{S_0} \mathrm{d}x \mathrm{d}y \int_0^{2\pi} \mathrm{d}\phi \int_0^1 \mathrm{d}\mu J(\boldsymbol{r}, \boldsymbol{\Omega}) \mu, \tag{27}$$

where $J(\boldsymbol{r}, \boldsymbol{\Omega}) = \int_{400\ \mathrm{nm}}^{700\ \mathrm{nm}} I_\lambda(\boldsymbol{r}, \boldsymbol{\Omega}) \mathrm{d}\lambda$ is the radiation intensity of the PAR irradiance streaming out of the sample stand in the upward direction $\boldsymbol{\Omega}$ and $I_\lambda(\boldsymbol{r}, \boldsymbol{\Omega})$ is a solution of the transport Eq. (1) at points of the canopy boundary. The forest albedo, A_F, can be written as

$$A_F = \lim_{S_0 \to \infty} E_F(S_0) / R_p \tag{28}$$

Our aim is to compare the forest albedo, A_F, and the assumed albedo, A_S, and to estimate their difference.

The radiation intensity, $J_S(\boldsymbol{\Omega})$, of the PAR irradiance captured by the sensor can be expressed via the radiation intensity of the PAR irradiance streaming out of the sample stand in the upward directions as (Fig. 9): $J_S(\boldsymbol{\Omega}) = J(\boldsymbol{r}_t, \mu, \phi)$, where $\boldsymbol{r}_t = \boldsymbol{r}_S - l[\boldsymbol{r}_S, \boldsymbol{\Omega}]\boldsymbol{\Omega}$ is a point on the top surface of the forest boundary; $l[\boldsymbol{r}_S, \boldsymbol{\Omega}]$

denotes the distance between the point $\boldsymbol{r}_S$ and the top surface of the forest boundary along the direction $-\boldsymbol{\Omega}$. We will express points of the surface δV_t in terms of polar coordinates with its pole at the point $O_S = (x_S, y_S, 0)$ and with the polar axes parallel to OX (Fig. 9). Let ρ_t and ϕ_t be the polar coordinates of a point $\boldsymbol{r}_t$ of the surface δV_t. The azimuth ϕ and the polar angle $\theta = \cos^{-1}\mu$ of the unit vector $\boldsymbol{\Omega}$ are:

$$\mu = \cos\theta = \frac{h}{\sqrt{h^2 + \rho_t^2}}, \quad \phi_t = \pi + \phi.$$

Substituting these equations in Eq. (25) and Eq. (27) we obtain:

$$E_S = \int_0^{2\pi}\int_0^{\infty} \frac{h^2\rho_t}{\left(h^2 + \rho_t^2\right)^2} J(O_S + \rho_t \boldsymbol{\Omega}_t; \mu, \phi)\,\mathrm{d}\phi_t\,\mathrm{d}\rho_t \tag{29}$$

$$E_F(S_0) = \int_0^{2\pi}\int_0^{\infty} \frac{h^2\rho_t}{\left(h^2 + \rho_t^2\right)^2} \left[\frac{1}{m(S_0)} \int\int_{S_0} J(O_S + r_t; \mu, \phi)\,\mathrm{d}r_t\right] \mathrm{d}\phi_t\,\mathrm{d}\rho_t, \tag{30}$$

where $\boldsymbol{\Omega}_t = (\cos\phi_t, \sin\phi_t, 0)$ is the unit vector (Fig. 9).

Eq. (29) depends on the space point O_S of the top canopy boundary. Its horizontal coordinates coincide with the horizontal coordinates of the sensor location. Eq. (30) is independent on this point because the integration in the square brackets is performed over all points of the surface S_0. Averaging Eq. (29) over points O_S and accounting Eqs. (26) and (28), we get the following relationship between the assumed albedo and the forest albedo:

$$\lim_{S_0 \to \infty} \frac{1}{m(S_0)} \int_{S_0} A_S\,\mathrm{d}O_s = A_F.$$

Thus, the forest albedo is equal to the mean assumed albedo, which results from averaging the responses of 'a large number of sensors' distributed over a horizontal surface above the forest canopy. If, therefore, a forest stand can be idealised as a horizontally homogeneous medium (i.e., $J(\boldsymbol{r}_t, \boldsymbol{\Omega})$ does not depend on points $\boldsymbol{r}_t$ of the top forest boundary) then, as it follows from Eqs. (29) and (30), the assumed albedo coincides with the forest albedo. In reality, however, such an idealisation is usually unrealistic. To illustrate, we evaluate the assumed and forest (Eqs. (29) and (30)) albedos by means of our three-dimensional model and compare these results with a measured assumed albedo.

The sample stand described in Section 3.1 and plotted in Fig. 1 was chosen to realise this experiment. Two PAR sensors were mounted 10 m above our forest canopy ($h = 10$) at the height $Z_S + h = 39$ m to measure the incident (R_p) and reflected ($E_{S,M}$) PAR energy fluxes. A clear sunny day (14 October 1994) was chosen to carry out these measurements. Dimensions of the simulated forest stand were $X_S = 25$ m and $Y_S = 30$ m in our calculations. Because our model simulates the radiative field in a forest of θfinite size, we approximate Eq. (29) by

$$E_S \approx \int_0^{\rho_0}\int_0^{2\pi} \frac{h^2\rho_t}{\left(h^2 + \rho_t^2\right)^2} J(O_S + \rho_t \boldsymbol{\Omega}_t; \mu, \phi)\,\mathrm{d}\rho_t\,\mathrm{d}\phi_t + \int_{\rho_0}^{\infty}\int_0^{2\pi} \frac{h^2\rho_t}{\left(h_2 + \rho_t^2\right)^2} J_M\,\mathrm{d}\rho_t\,\mathrm{d}\phi_t$$

$$= E_{S,0}(\rho_0) + \pi J_M \frac{h^2}{h_2 + \rho_0^2} \tag{31}$$

where $E_{S,0}(\rho_0)$ denotes the first integral term and J_M is the value of mean intensity of PAR energy reflected by the top forest boundary δV_t, of dimensions $X_S = 25$ m and $Y_S = 30$ m and captured by the sensor, i.e., $\pi J_M = E_{S,0}(\rho_0)$. The value ρ_0 was chosen so that $\pi\rho_0^2 = X_S Y_S$, i.e., $\rho_0 = 15.5$ m.

Fig. 10 shows the diurnal variation of the assumed albedo derived from measurements ($A_{S,M}(t) = E_{S,M}/R_p$)

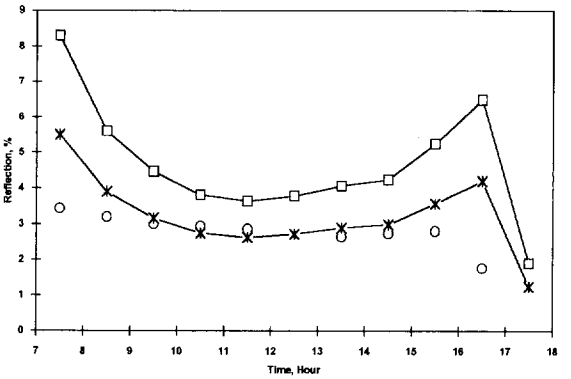

Fig. 10. Diurnal variation of forest albedo obtained by measurements (○), by adjusted measurements (*), and by model calculations (□).

and from simulations ($A_S(t) = E_S/R_p$). The diurnal variation of the forest albedo, $A_F(S_0,t) = E_A(S_0)/R_p$, is plotted in this figure also. The top canopy boundary, δV_t, was taken as S_0 (see Eq. (27)) in our calculations. A difference between the diurnal variation of the simulated sensor and forest albedos makes up 45%. This difference was derived from Eq. (19) in which $M(t)$ and $M_S(t)$ are replaced by $A_S(t)$ and $A_F(S_0,t)$ respectively. Note that Eq. (19) took the value 18% for transmitted and spatially averaged radiation on a clear sunny day. The radiant energy that penetrated through the forest canopy and captured by a sensor located under-crown space is also described by Eq. (29), in which the angular variable μ must be replaced by $-\mu$ and the spatial variable by points on a under-crown surface. The sensor response, therefore, strongly depends on its location in the forest and is characterised by a large spatial variation in both these cases. Its spatial average, e.g., as it was shown in Section 3.3, is needed to evaluate both an amount of transmitted radiation and the forest albedo correctly.

The diurnal mean of the simulated assumed and forest albedos were 3.1% and 4.5%, respectively. Evaluation of the forest albedo by diurnal mean response of one fixed sensor above the forest stand does not determine the average of the forest heterogeneity. In our example, the difference makes up 45% with respect to the sensor response.

The difference between the diurnal variation of the measured assumed albedo, $A_{S,M}(t)$, and the simulated $A_S(t)$, as it was derived from Eq. (19), is 25%. This difference is mainly caused by inaccuracies in the evaluation of radiant energy intercepted by the sensor during the early morning and the late evening hours. We think that our model evaluates the sensor response more accurately than it provides a real sensor. This hypothesis is based on the following arguments. It follows from Eq. (31) that the radiant energy reflected by the forest and captured by the sensor can be represented by the sum of two components. The first, $E_{S,0}(\rho_0)$, is the radiant energy that reaches the sensor at the angles between 0 and $\theta_0 = \cos^{-1}\left(h/\sqrt{h^2+\rho_0^2}\right)$ to the upward normal of the sensor surface, and the second component is the radiant energy reaching the sensor from other directions. The real sensor can register radiant flux that exceeds a critical value of sensor sensitivity, ϵ, i.e. when $\pi J_M h^2/(h^2+\rho_0^2) > \epsilon$. It follows from this inequality that the decrease of J_M involves decreasing the angle θ_0. Because the incoming PAR radiation is small during the early morning and the late evening hours, the mean intensity of scattered PAR radiation J_M is also small and, as a consequence, the sensor can measure the radiant flux reaching the sensor from small solid angle about the upward normal to the sensor surface. As a result, a fraction of a scattered PAR energy is not registered by the sensor. Note at a low solar elevation, the direction of scattered PAR energy caused by the hot spot is also low. This energy, therefore, may not be registered by the sensor in spite of the fact that the intensity of scattered radiation reaches its maximum about hot spot directions (Kuusk, 1991). Clearly these arguments do not precisely prove our hypothesis about the

sensor response during the early morning and the late evening hours. However, the problem of evaluating a correct value of the forest PAR albedo needs special attention.

7. Conclusions

We used the transport theory to simulate three-dimensional radiative field. This theory is based on assumption that Beer's law can be locally applied to describe light interaction with a plant canopy (Ross, 1981) that holds true for sufficiently great volumes filled with phytoelements. It predetermines a spatial scale at which this approach is applicable.

Forest structure models accounting for the tree shapes, their spatial locations and the vertical distribution of foliage elements within each individual crown can be appropriate to predict mean energy fluxes over horizontal surfaces. The mean energy fluxes over a horizontal area of about 10×1 m^2 below the forest canopy is underestimated by our model by about 20–25%. The length of this surface was slightly greater than a maximum diameter of crown projections. These predicted fluxes in such models are mainly caused by the radiant interaction with a thin layer of tree crowns and with the soil in between-crown openings. They are only slightly sensitive to the within-crown radiative regime. Such structural models, therefore, are well justified to predict the radiation reflected by the tree crown, but may lead to essential miscalculation of the photosynthesis process. The canopy photosynthesis results from the interaction between the distribution of radiation on the foliage and the photosynthetic response of foliage elements. Therefore, the evaluation of mean radiant energy over surfaces of different inclinations is needed to model canopy photosynthesis correctly. This can be achieved if the forest structure model provides the distribution of phytoelements over surfaces of different inclinations with the necessary degree of accuracy.

Ignoring the spectral composition of the incoming solar radiation and the spectral variation of leaf reflectance and transmittance can lead to an essential overestimation of the PAR energy fluxes at a lower crown level. According to our estimates, such a difference can reach 26%. A special submodel for retrieving the spectral composition of the incoming radiation from the direct PAR beam incident at the forest canopy is, therefore, incorporated into our canopy-radiation model.

A neighbouring environment may influence the radiative regime in a forest canopy of a small area. This influence is more pronounced during cloudy days than during clear sunny days. A special technique was realised in our model to account for the effect of the forest surroundings on the canopy radiative regime. It makes it possible to use our model for evaluating the impact of various forest management methods on the solar energy available for forest growth and other ecosystem processes.

The response of a hemispherical PAR sensor installed above the forest canopy and registering an upward energy flux depends strongly on the sensor location. This dependence is mainly caused by forest heterogeneity. Diurnal mean response of one fixed sensor above the forest canopy does not average the effect of the forest heterogeneity. A special arrangement of several radiation sensors above the forest canopy is needed to measure the forest PAR albedo correctly. For example, a location of a PAR sensor (selected by chance) above a coniferous forest stand at the scientific research station 'Solling', near Göttingen (Germany), leads to an underestimation of the reflected PAR energy by 45%. This finding suggests that the radiation balance over the whole short- and long-wave frequency distribution could be overestimated, an indicator that is often found in field measurements (Laubach et al., 1994; Laubach, 1995). A strict argument or a disproof of this hypothesis, however, needs special investigation.

Acknowledgements

Yuri Knyazikhin and Oleg Panfyorov were supported by the Federal Ministry for Education, Germany, through Grant No. 0339474B 'Veränderungsdynamik von Waldökosystem'. We gratefully acknowledge this support.

References

Bass, L.P., Volocsvhenko, A.M., Germogenova, T.A., 1986. Methods of discrete ordinates in radiation transport problems. Inst. Appl. Mathem., USSR Academy of Sci., Moscow, 231 pp. (in Russian, with English abstract).

Borel-Donohue, C.C., 1988. Models for back scattering of millimeter waves from vegetative canopies. PhD Thesis, Dept. Electrical and Computer Eng., Univ. of Massachusetts at Amherst, MA, 01003.

Borel, C.C., Gerstl, S.A.W., Powers, B., 1991. The radiosity method in optical remote sensing of structured 3-D surfaces. Remote Send. Environ. 36, 13–44.

Carlson, B.G., 1970. Transport theory: discrete ordinates quadrature over the unit sphere. LANL Rep. LA-4554, Los Alamos Natl. Laboratory.

Constantin, J., 1993. Stoffeinträge in ein Fichtenwaldökosystem durch Deposition luftgetragener Partikel und Nebeltröpfchen. Berichte des Forschungszentrum Waldökosysteme, Göttingen, Reihe A., Bd. 106, 165 pp.

de Reffye, Ph., Dinouard, P., Barthélémy, D., 1991. Modélisation et simulation de l'architecture de l'orme du japonZelkovaSerrata (Thunb.) Makino (Ulmaceae): La notion d'axe de référence. Naturalia Monspeliensia, h.s., Montpellier, 251–266.

Ellenberg, H., Mayer, R., Schauermann, J., 1986. Ökosystemforschung: Ergebnisse des Sollingprojekts. Eugen Ulmer Verlag, Stuttgard.

Germogenova, T.A., 1986. The Local Properties of the Solution of the Transport Equation. Nauka, Moscow, 272 pp. (in Russian).

Goel, N.S., 1988. Models of vegetation canopy reflectance and their use in estimation of biophysical parameters from reflected data. Remote Sens. Rev. 4, 1–213.

Hall, G., Watt, J.M. (Eds.), 1976. Modern Numerical Methods for Ordinary Differential Equations. Clarendon Press, Oxford, 204 pp.

Ibrom, A., 1993. Die Deposition und die Pflanzenauswaschung (Leaching) von Pflanzennährstoffen in einem Fichtenbestand im Solling. Berichte des Forschungszentrum Waldökosysteme, Göttingen, Reihe A., Bd. 105, 165 pp.

Kimes, D.S., 1991. Radiative transfer in homogeneous and heterogeneous vegetation canopies, In: Myneni, R.B., Ross, J. (Eds.), Photon-Vegetation Interactions: Applications in Plant Physiology and Optical Remote Sensing. Springer, Berlin, pp. 339–388.

Knyazikhin, Yu., Marshak, A., 1991. Fundamental equations of radiative transfer in leaf canopies and iterative methods for their solution. In: Myneni, R.B., Ross, J. (Eds.), Photon-Vegetation Interactions: Applications in Plant Physiology and Optical Remote Sensing. Springer, Berlin, pp. 9–43.

Knyazikhin, Yu.V., Marshak, A.L., Myneni, R.B., 1992. Interaction of photons in a canopy of finite-dimensional leaves. Remote Sens. Environ. 39, 61–74.

Knyazikhin, Yu., Marshak, A., Schulze, D., Myneni, R., Gravenhorst, G., 1994. Optimization of solar radiation input in forest canopy as a tool for planting/cutting of trees. Transport Theory and Statist. Phys. 5, 671–700.

Knyazikhin, Yu., Kranigk, J., Miessen, G., Panfyorov, O., Vygodskaya, N., Gravenhorst, G., 1996. Modelling three-dimensional distribution of photosynthetically active radiation in Sloping coniferous stands. Biomass and Bioenergy 2–3, 189–200.

Kondratyev, K.Ya., 1969. Radiation in the Atmosphere. Academic Press, New York, 912 pp.

Kranigk, J., 1996. Ein Model für den Strahlungstransport in Fichtenbeständen. Cuvillier Verlag, Goettingen, 127 pp.

Kranigk, J., Gruber, F., Heimann, J., Thorwest, A., 1994. Ein Model für die Kronenraumstruktur und die räumliche Verteilung der Nadeloberfläche in einem Fichtenbestand. Allg. Forst-u.J.-Ztg., 165., Jg. 10–11, 193–197.

Kranigk, J., Gravenhorst, G., 1993. Ein dreidimensionales Modell für Fichtenkronen. Allg. Forst-u.J.-Ztg., 164., Jg. 8, 146–149.

Kurth, W., 1994. Morphological models of plant growth: possibilities and ecological relevance. Ecol. Modell. 75–76. 299–308.

Kuusk, A., 1991. The hot spot effect in plant canopy reflectance. In: Myneni, R.B., Ross, J. (Eds.), Photon–Vegetation Interactions: Applications in Plant Physiology and Optical Remote Sensing. Springer, Berlin, pp. 139–159.

Larsen, D.R., Kershaw, J.A. Jr., 1996. Influence of canopy structure assumption on predictions from Beer's law. A comparison of deterministic and stochastic simulation. Agric. For. Meteorol. 81, 61–67.

Laubach, J., 1995. Charakterisierung des turbulenten Austauschs von Wärme, Wasserdampf und Kohlendioxid über niedriger Vegetation anhand von Eddy-Korrelations-Messungen. PhD Thesis, Universität Leipzig, Leipzig, Germany, 139 pp.

Laubach, J., Raschendorfer, M., Kreilein, H., Gravenhorst, G., 1994. Determination of heat and water vapour fluxes above a spruce forest by eddy correlation. Agric. For. Meteorol. 71, 373–401.

Li, X., Strahler, A.H., 1986. Geometrical–optical bidirectional reflectance modeling of a conifer forest canopy. IEEE Trans. Geosci. Remote Sens. 24, 906–919.

Monsi, M., Saeki, T., 1953. Über den Lichtfaktor in den Pflanzengesellschaften und seine Bedeutung für die Stoffproduktion. Jap. J. Bot. 14, 22–52.

Monteith, J.L., Unsworth, M.H., 1990. Principles of Environmental Physics. E. Arnold, London, 291 pp.

Myneni, R.B., 1991. Modeling radiative transfer and photosynthesis in three-dimensional vegetation canopies. Agric. For. Meteorol. 55, 323–344.

Myneni, R.B., Asrar, G., Gerstl, S.A.W., 1990. Radiative transfer in three-dimensional leaf canopies. Transport Theory and Stat. Phys. 19, 205–250.

Myneni, R.B., Marshak, A., Knyazikhin, Yu., Asrar, G., 1991. The method of discrete ordinates. In: Myneni, R.B., Ross, J. (Eds.), Photon–Vegetation Interactions: Applications in Plant Physiology and Optical Remote Sensing. Springer, Berlin, pp. 45–109.

Norman, J.M., Welles, J.M., 1983. Radiative transfer in an array of canopies. Agron. J. 75, 481–488.
Nilson, T., 1992. Radiative transfer in nonhomogeneous plant canopies. In: Stanhill, G. (Ed.), Advances in Bioclimatology 1. Springer, Berlin, pp. 59–88.
Oker-Blom, P., 1986. Photosynthetic radiation regime and canopy structure in modelled forest stands. Acta For. Fenn. 197, 1–44.
Oker-Blom, P., Kellomäki, S., 1983. Effect of grouping of foliage on within-stand and within-crown light regime: comparison of random and grouping canopy models. Agric. For. Meteorol. 28, 143–155.
Pokrowski, G.I., 1929. Über die Helligkeitsverteilung am Himmel. Physikal. Zeitschr. 30, 697–700.
Riederer, M., Kurbasik, K., Steinbrecher, R., Voss, A., 1988. Surface areas, lengths and volumes of *Picea abies* (L.) Karst. needles: determination, biological variability and effect of environmental factors. Trees 2, 165–172.
Ross, J., 1981. The Radiation Regime and Architecture of Plant Stands. Dr. W. Junk Publ., The Hague, Netherlands, 391 pp.
Ross, J., Knyazikhin, Yu., Kuusk, A., Marshak, A., Nilson, T., 1992. Mathematical Modeling of the Solar Radiation Transfer in Plant Canopies. Gidrometeoizdat, St. Peterburg, 195 pp. (in Russian, with English abstract).
Ross, J.K., Marshak, A.L., 1984. Calculation of solar radiation reflection from plant cover using the Monte-Carlo method. Sov. J. Remote Sens. 5, 58–67, in Russian, translated into English.
Ross, J., Meinander, O., Sulev, M., 1994. Spectral scattering properties of scots pine shoot. In.: Int. Geosci. and Remote Sens. Symp. (IGARS '94). Inst. Techn. Pasadena, CA, USA, August 1994, Vol. 2, 1451–1454.
Ross, J., Nilson, T., 1968. A mathematical model of radiation regime of plant cover. In: Actinometry and Atmospheric Optics. Valgus. Tallin (in Russian).
Smith, N.J., 1993. Estimating leaf area index and light extinction coefficients in stands of Douglas-fir (*Pseudotsuga menziesii*). Can. J. For. Res. 23, 317–321.
Smolander, H., Stenberg, P., Linder, S., 1994. Dependence of light interception efficiency of Scots pine shoots on structural parameters. Tree Physiol. 14, 971–980.
Stenberg, P., Linder, S., Smolander, H., Flower-Ellis, J., 1994. Performance of the LAI-2000 canopy analyzer in estimating leaf area index of some Scots pine stands. Tree Physiol. 14, 981–996.
Stenberg, P., 1995. Penumbra in within-shot and between-shoot shading in conifers and its significance for photosynthesis. Ecol. Modell. 77, 215–231.
Spitters, C.J.T., Toussain, H.A.J.M., Goudrian, J., 1986. Separating the diffuse and direct component of global radiation and its imolication for modeling canopy photosynthesis. Agric. For. Meteorol. 38, 217–229.
Tikhonov, A.R., Arsenin, V.Ya., 1979. Methods for Solution of Ill-posed Problems. Nauka. Moscow, 288 pp. (in Russian).
Vainikko, G., 1993. Multidimensional Weakly Singular Integral Equations. Lecture Notes in Math., V. 1549. Springer, 159 + XI p.
Vanderbilt, V.C., Grant, L., 1985. Plant canopy specular reflectance model. IEEE Trans. Geosc. Remote Sensing 23, 722–730.
Vedyushkin, M., 1995. Fractal characteristics of forest spatial structure. Vegetatio 113 (1), 65–70.
Vladimirov, V.V., 1963. Mathematical problems in the one-velocity theory of particle transport. AECL-1661, Chalk, River, Ontario, Canada.
Wang, Y.P., Jarvis, P.G., 1990. Description and validation of an array model—MAESTRO. Agric. For. Meteorol. 51, 257–280.
Zeide, B., Pfeifer, P., 1991. A method for estimation of fractal dimension of tree crowns. Forest Sci. 5, 1253–1265.